Title

Hippocampal cells multiplex positive and negative engrams

Authors

Monika Shpokayte[1,5], Olivia McKissick[2], Bingbing Yuan[3], Bahar Rahsepar[4,5], Fernando R. Fernandez[4,5], Evan Ruesch[5,], John A. White[4,5], X. Shawn Liu[6*], Steve Ramirez[4,5*]

Affiliations

[1]Graduate Program for Neuroscience, Boston University, Boston, MA, 02215

[2]Neuroscience Graduate Program, Brown University, Providence, RI, 02912

[3]Whitehead Institute for Biomedical Research, MIT, Cambridge, MA, 02142

[4]Department of Biomedical Engineering, Boston University, Boston, MA, 02215

[5]Department of Psychological and Brain Sciences, The Center for Systems Neuroscience, Neurophotonics Center, and Photonics Center, Boston University, Boston, MA, 02215

[6]Department of Physiology and Cellular Biophysics, Columbia University Medical Center, New York, NY 10032

*Corresponding Author

One sentence summary

The hippocampus contains neurons that correspond to positive and negative engrams, which are segregated by their molecular, cellular, and projection-specific features

Abstract

The hippocampus is involved in processing a variety of mnemonic computations specifically the spatiotemporal components and emotional dimensions of contextual memory.[1-3] Recent studies have demonstrated vast structural and functional heterogeneity along the dorsal-ventral axis[1,5] of the hippocampus, and while much is known about how the dorsal hippocampus processes spatial-temporal content, much less is known about whether or not the ventral hippocampus (vHPC) partitions positive and negative experiences into distinct sets of cells.[4-9] Here, we combine transgenic and all-virus based activity-dependent tagging strategies to visualize multiple valence-specific engrams in the vHPC and demonstrate two partially segregated cell populations and projections that respond to positive and negative experiences. Next, using an RNA sequencing approach, we find that vHPC positive and negative engram cells display distinct transcriptional programs compared to a neutral engram population. Additionally, while optogenetic manipulation of tagged cell bodies in vHPC is not sufficient to drive preference or avoidance, stimulation of tagged vHPC terminals projecting to the amygdala and nucleus accumbens (NAc), but not the prefrontal cortex (PFC), drives preference and avoidance. These terminals can also undergo a "switch" or "reset" in their capacity to drive either, thereby demonstrating their flexible contributions to behavior. We conclude that the vHPC contains genetically, cellularly, and behaviorally distinct populations of cells processing positive and negative memory engrams. Together, our findings provide a novel means by which to visualize multiple engrams within the same brain and point to their unique genetic signatures as reference maps for the future development of new therapeutic strategies.

Within the brain we find a rich repository of memories that can be imbued with positive and negatively valenced information. These experiences leave enduring structural and functional changes that are parceled up into discrete sets of cells and circuits comprising the memory

engram[10]. Recent studies have successfully visualized and manipulated defined sets of cells previously active during a single experience[10-17]. However, how multiple engrams of varying valences (hereafter defined as cells that differentially respond to positive or negative events in a stimulus-independent manner[18]) are represented within the same brain region remains poorly understood. Previous studies have suggested the ventral hippocampus (vHPC) selectively demarcates and relays emotional information to various downstream targets. We sought to characterize the molecular and cellular identities and the behaviorally-relevant functions of vHPC cells processing positive and negative engrams, with a focus on ventral CA1 (vCA1). In order to address the question of how the vCA1 processes multiple emotional experiences, we first devised a strategy combining two cFos-based tagging methods with endogenous cfos immunohistochemistry to visualize engrams across three discrete timepoints. First, we then anatomically charted the projection patterns of positive and negative-tagged vCA1 cells to measure structural overlap and segregation across various downstream targets. Second, we performed large-scale RNA sequencing (RNA-seq) to investigate the genetic features of these sets of cells. Lastly, we behaviorally tested the causal role and functional flexibility vHPC cells in both a cell body and projection-specific manner.

First, to access cells across multiple timepoints and in an activity-dependent, within-subject manner, we used the Fos-based transgenic animal, TRAP2[18], under the control of 4-Hydroxytamoxifen (4-OHT) paired with an all-virus Fos-based strategy under the control of doxycycline[10] (Dox) (Fig. 4a). TRAP2+ mice expressing iCre-ERT2 recombinase, when injected with DMSO instead of 4-OHT, show no TdTomato expression (Extended Data Fig. 1), were injected bilaterally with a cocktail of viruses: AAV9-Flex-DIO-TdTomato and AAV-cFos-tTA + AAV-TRE-EYFP. The cfos-tTA strategy couples the *c-Fos* promoter to the tetracycline

transactivator (tTA), which, in its protein form, directly binds to the tetracycline response element (TRE) in a doxycycline-(Dox)-dependent manner and drives the expression of a protein of interest (i.e. EYFP). Combining these two independent systems yields two inducible windows for tagging vHPC cells within the same subject (See Methods).

After injecting the aforementioned virus cocktail into the vHPC, we used this "dual tagging" system to label cells processing positive or negative engrams. Ten days after surgery and recovery, mice were taken off their DOX chow diet for 48 hours to open the first window of tagging. While off DOX, the mice were subjected to female exposure for 1 hour in a clean homecage[13, 20] and placed immediately back on the DOX diet for the remainder of the study. To tag the second set of cells, 24 hours later male mice were subjected to four 2 second 1.5mA foot shocks. 30 minutes after the end of fear conditioning, the mice were injected with 40mg/kg of 4-OHT and left undisturbed for 72 hours (Fig. 1b). We first observed a striking anatomical distinction between positive and negative engrams along the anterior and posterior axis in sagittal sections of vCA1 (Fig. 1c). Positive engram cells were predominantly located in more posterior sections, whereas, negative engram cells were largely present in anterior sections of vCA1, with a salt-and-pepper pattern observed within medial sections (Fig. 1c-d).

Next, using the same dual tagging strategy as above, we asked whether or not these positive- and negative-tagged populations were recruited during subsequent experiences of similar valences. To that end, we added a third time point by visualizing endogenous cFos expression 90 minutes after a final behavioral experience, i.e. exposure to sweetened condensed milk or restraint stress[19] (Fig. 1e-f). To control for the order experiences, we counterbalanced four groups, each which contained two tagged populations of cells (i.e. "negative" for cells tagged by fear conditioning and "positive"

for cells tagged by male-female interactions), followed by a third experience of varying valence (i.e. restraint stress or sweetened condensed milk) which was captured by endogenous cFos expression. Our groups were as follows: Negative-Positive-Restraint Stress (GROUP 1), Negative-Negative-Restraint Stress (GROUP 2), Positive-Negative-Sweetened Condensed Milk (GROUP3), and Positive-Positive-Sweetened Condensed Milk (GROUP 4). In each group we measured the cellular co-localization of TdTomato, EYFP, and cFos to infer which cells were active in one or more of the three experiences (Fig. 1g). All mice exhibited a similar proportion of tagged cells across all three tagging approaches regardless of valence or method of tagging (Fig. 1h).

Histological analyses revealed that there were significantly higher rates of cells showing co-localization of TdTomato and EYFP when labelled with the same experiences (i.e. positive and positive) and lower rates of co-localization when labeling differently valenced experiences (i.e. Positive and negative; Fig. 1i). Further, we observed significant colocalization between TdTomato, EYFP, and cFos when mice were subjected to three negative or three positive experiences, i.e. GROUP 2 and GROUP 4 respectively. Positive-tagged cells were preferentially reactivated when mice were exposed to sweetened condensed milk, and negative-tagged cells were preferentially reactivated when mice were exposed to restraint stress (Extended Data Fig. 2 & Fig. 3). Together, these findings raise the intriguing possibility that vCA1 designates emotionally-relevant information to two partially non-overlapping sets of cells.

Next, we used the same dual-tagging strategies to characterize the basic physiological properties of vHPC cells (Extended Data Fig. 4). TRAP2 mice were co-injected with the same activity

dependent viruses and tagged in the same manner as mentioned previously (Extended Data Fig. 4a-b). Interestingly, we did not observe any differences in firing frequency, suprathreshold characterization, adaptation rate, input rate, or spike rates (Extended Data Fig. 4c-l) suggesting that, despite recruiting partially non-overlapping sets of cells for positive and negative experiences, these tagged cells themselves share similar physiological characteristics.

Despite these physiological similarities, vHPC cells have been shown to project to a myriad of distinct brain regions involved in stress and approach-avoidance behaviors, thereby forming multi-regional networks involving emotion and memory[1]. We speculated that within these networks there exists structural heterogeneity partly defined by whether an experience is positively or negatively valenced, as has been observed in areas including the amygdala[10,25,27], nucleus accumbens[29], and medial prefrontal cortex[36]. Using our dual tagging strategy, we next traced vHPC outputs tagged by positive or negative experiences in a within-subject manner and measured the axonal fluorescence intensities in the following target areas, given their crucial role in emotional processing: BLA, NAc, PFC, dorsal hypothalamus, fornix, and the dentate gyrus. Interestingly, we observed partial overlap between positive and negative-tagged vCA1 terminals in the medial BLA (A.P. -1.8) and the PFC (including IL and PL), while also finding evidence of structural segregation in the following regions: we observed predominantly stronger EYFP (positive) projections, as measured by fluorescence intensities, to the basomedial amygdala Posterior part (BMP), anterior commissure anterior part (ACA), fornix, dorsal medial hypothalamic nucleus (DMD and DMV), and the lower layer of the dentate gyrus. Further, we found predominantly stronger TdTomato (negative) projections to the anterior BLA, posterior BLA, NAc core, and the

upper layer of the DG. (Fig. 2 and Extended Data Fig. 5). Previous studies have demonstrated that neurons in regions such as the PFC[36], NAc[29], and BLA[10.25], collectively process experiences in a manner that can be anatomically segregated or heterogeneous. We posit that positive- and negative-tagged vHPC terminals are embedded in a larger network of emotional memory processing that can be partly defined both by unique anatomical patterns and by the activity-dependent recruitment of ensembles involved in processing a specific valence.

Recent studies have identified unique molecular profiles of vCA1 cells containing distinct projection targets. These vCA1 projections transmit information to multiple areas involved in emotion and memory and form a network that can be organized by unique architectural features, including vCA1 cell inputs, outputs, and transcriptional signatures[1]. Accordingly, we next asked whether or not the molecular composition of vHPC cells contained distinct genetic profiles. To catalogue the molecular landscape of vHPC cells in an activity- dependent manner, we tagged a positive experience (i.e. male-female interactions), a negative experience (i.e. multiple shocks), or a neutral experience (i.e. exposure to the same conditioning cage without positive or negative stimuli; see methods; Fig. 3a). We thenperformed RNA-seq using tagged nuclei (EYFP+) isolated by Fluorescence-Activated Cell Sorting (FACS), which showed 0.5~0.6% tagged nuclei from each group (Fig. 3c). Comparing negative and positive vCA1 cells to the neutral group, we identified 474 differentially expressed genes (DEGs) in negative vCA1 cells (Fig. 3d and 3f), including 340 down regulated genes and 134 upregulated genes (Fig. 3g). We also identified 1,104 DEGs in positive vCA1 cells compared to the neutral group (Fig. 3e and 3f), including 1,025 down regulated genes and 79 upregulated genes (Fig. 3g). There were 842 unique DEGs in positive engram cells

and 212 unique DEGs in negative engram cells (Fig. 3f), suggesting distinct transcriptional landscapes in these two populations. Furthermore, the top 20 upregulated and downregulated DEGs identified for negative and positive vCA1 cells showed no overlap with each other (Fig. 3d and 3e, Table S1 and S2), supporting the distinct transcriptomes in these neurons. Interestingly, among these DEGs we identified one gene ***NUFIP1*** (Nuclear Fragile X Mental Retardation Protein Interacting Protein 1) that was upregulated in positive engram and downregulated in negative engram (Fig. 3g). This gene encodes a nuclear RNA binding protein that contains a C2H2 zinc finger motif and a nuclear localization signal[47]. Diseases associated with NUFIP1 mutations include Peho Syndrome (progressive encephalopathy with Edema, Hypsarrhythmia and Optic atrophy), an autosomal recessive and dominate, progressive neurodegenerative disorder that starts in the first few weeks or months of life. Its interacting protein FMRP1 is essential for protein synthesis in the synapse[48] and CGG trinucleotide expansion mutation of FMR1 gene coding FMRP1 cause Fragile X syndrome, the most common intellectual disability in males[49]. Further investigation of the functional significance of NUFIP1 and other DEGs could reveal mechanistic insights to the trancriptomic plasticity engaged by the valences of memory.

To gain deeper insight into the molecular signatures of transcriptomes associated with negative and positive vCA1 cells, we performed Gene Ontology (GO) analysis of the up- and down-regulated pathways in negative and positive vCA1 cells (Fig. 3h-k). We found that the top upregulated pathway in negative engram cells involved neurotransmitter complexes such as ionotropic glutamate receptor activity (Fig. 3h). This finding is consistent with previous studies using brain tissues that identified 3,759 differentially methylated DNA regions in the hippocampus

associated with 1,206 genes enriched in the categories of ion gated channel activity after contextual fear conditioning[48,50,51]. Interestingly, we found the top downregulated pathway in negative engram cells involved DNA mismatch repair (Fig. 3i). Although the top upregulated pathways in positive engram cells also include ionotropic glutamate receptor activity (Fig. 3j), the top downregulated pathways in positive engram cells enrich on axoneme assembly and microtubule bundle formation (Fig. 3k) different from the pathways downregulated in positive engram cells (Fig. 3i). Next, we compared the RNA-seq data between positive and negative engram cells directly. We identified 494 DEGs, including 47 upregulated genes and 447 downregulated genes (Extended Fig. 6a). Furthermore, we found that five pathways were upregulated in positive vCA1 cells such as nuclear exosome RNAse complex and 16 pathways were down regulated in positive engram compared to negative vCA1 cells, such as axoneme assembly (Extended Fig. 6b and 6c). These differentially altered signaling pathways between negative and positive vCA1 cells, which resulted from multiple comparisons, support our conclusion that these neurons indeed represent transcriptionally distinct subpopulations.

Finally, to test for a causal role of tagged vHPC cell bodies and its selected terminals in driving behavior, we infused a virus cocktail of AAV9-cFos-tTA and AAV9-TRE-ChR2-EYFP or AAV9-TRE-EYFP into vCA1. We then implanted an optical fiber bilaterally above either the vCA1 or its terminals, vCA1–BLA, vCA1–NAc, vCA1–PFC (Fig. 4a). We first found that all terminals were capable of activating their corresponding downstream targets by assessing increases in cFos levels following stimulation (Extended Data Fig. 7). Following 10 days of recovery, a separate group of mice were taken off DOX and tagged with negative (i.e. shock) or positive (i.e. male-female

interactions) experiences. For the first set of experiments, on Day 1, the negatively tagged mice were placed in a real-time place preference/avoidance (RTPP/A) chamber on day 1 to assess baseline levels (Fig. 4b). On day 3, the animals were placed back into the PTPP/A chamber; this time they received optical stimulation at 20Hz bilaterally on one side and no stimulation on the other. We found that optical stimulation of vCA1–BLA or vCA1–NAc terminals drove aversion (Fig 4e & f), whereas the EYFP controls, vCA1 cell body stimulation, and vCA1-PFC terminals did not statistically deviate from baseline levels (Fig 4c, d, & g). On day 5 of the experiment, the mice were subjected to an induction protocol, as previously reported[13], to test the capacity of the engram to "switch" the behavior it drives. The negative-tagged male mice were placed in a new chamber with a female mouse for 10 minutes while receiving optical stimulation for the entire duration of exposure. Afterwards, the animals were placed back in their chambers and assessed for behavioral changes on day 7. In this post-induction test, we observed that optical stimulation of vCA1–BLA terminals was now sufficient to drive preference despite driving aversion in the pre-induction test earlier (Fig. 4e). The induction protocol also revealed that vCA1–NAc terminals, which previously were sufficient to drive aversion, now had reversed or "reset" their capacity to modulate behavior and returned to baseline levels (Fig. 4g). Lastly, we saw no changes in the EYFP controls, vCA1 cell body, or vCA1–PFC stimulation (Fig 4c, d, & g).

Next, we asked whether positive-tagged vCA1 terminals to the BLA, NAc, or PFC were sufficient to modulate behavior (Fig 4h). Similar to the above findings, optical stimulation of vCA1–BLA (Fig. 4k) and vCA1-NAc (Fig. 4l) terminals, but not in any of the other groups (Fig. 4i, j, &m), was sufficient to drive place preference. During the induction phase of the experiment, we placed

the mice into a fear conditioning chamber where they received multiple foot shocks and simultaneous optical stimulation of the positive-tagged terminals. This experiment assessed if these vCA1 terminals are able to "switch" or "reset" their capacity to drive preference in a manner mirroring the experiments above. Indeed, we found that in the post-induction tests, the vCA1–BLA group switches from driving preference to aversion (Fig. 4k) while the vCA1–NAc group resets from driving preference back to baseline levels (Fig. 4l). Furthermore, we did not observe this effect in neutral-tagged animals (Extended Data Fig. 8), nor did we see any statistically significant behavioral changes for the RTPP/A task in the EYFP controls, vCA1 cell body stimulation group, or vCA1–PFC stimulation group (Fig. 4i, j, &m). Importantly, we tested whether optical stimulation may cause increases in motor behaviors. We found no significant difference in distance travelled across all groups during light on or off epochs in an open field (Extended Data Fig. 9). Moreover, the lack of preference or avoidance observed from vCA1 cell body stimulation raised the possibility that vCA1's role in driving behavior is determined in a terminal-specific manner[24]; a notion that dovetails with recent studies suggesting that computations along the axons of a given cell body can differentially drive behavior in accordance with the downstream target[8]. Taken together, these results suggest that vHPC cell bodies relay their behaviorally-relevant and valence specific content to its downstream targets despite sharing partially non-overlapping molecular and neuronal signatures and distinct projection patterns. This is corroborated by evidence showing that vHPC axonal outputs preferentially route independent features of a given behavior[7].

Here we have shown that the vHPC processes positive and negative experiences in defined populations of cells that are partially distinct at the molecular, cellular, and projection-specific levels. We also demonstrated their capacity to drive behaviors through functionally plastic projection-specific terminals. Our immunohistochemical data suggest that vCA1 contains at least three populations of neurons: two subsets that can be demarcated based on their anterior-posterior locations and preferential response to positive or negative valences, and a third population that responds to both, perhaps reflecting a biological predilection for salience.[5] While their exact brain-wide structural and functional outputs remain undetermined, we speculate that our observed population of vCA1 cells responding to fear are a superset of recently observed anxiety cells that transmit information to the hypothalamus[27] and PFC[28]. Moreover, vCA1 cells processing fear and/or reward perhaps route information to and innervate the BLA and NAc at differing anatomic, receptor- and cell-type specifically optimizing their capacity to integrate mnemonic information[27].

Additionally, by combining transgenic activity-dependent tagging strategies with all-virus-based expression of fluorophores, our design permits the visualization of multiple ensembles in a within-subject manner, which coalesces with previous studies monitoring and manipulating a single ensemble active at two discrete time points as well[29]. By intersecting these approaches with genetic sequencing strategies, these tools enable the tagging, manipulation, and molecular documentation of cells processing fear and reward opening the possibility of cataloguing topographical similarities and differences between the two in a brain-wide manner. For instance, future studies may probe the molecular composition of positive- and negative-tagged vCA1 cells along its anterior-posterior axis, and test whether or not the transcriptomic profiles of these cells differs both

across valence and their physical location. Moreover, it is intriguing that vCA1 positive- and negative-tagged terminals showed evidence of segregation within the amygdala and hippocampus. Consequently, subsequent research may seek to functionally tease out their contributions to behavior, ands measure the types of information they are transmitting through a combination of imaging and terminal-specific perturbation approaches.

It is important to constrain interpretations of engrams given the vast array of genetic tools used to access cells in an activity-dependent manner. For instance, vCA1 ensembles vary drastically in size and in activity patterns across learning and memory. These numbers range from single percentages and can reach ~35% of cells depending on immediate early gene marker used, tagging strategy, rodent line, and viral tools employed[32-35]. Fittingly, we believe that our dual-tagging strategy partly over-samples the number of tagged cells given the time-frame necessary for tagging to occur (e.g. 48 hours off Dox; 72 hours post-4OHT injection[37-40]), and future experiments may aim to improve the temporal resolution of contemporary tagging approaches to enhance the signal-to-noise ratio of experience-related tagging to background tagging or leakiness. Additionally, cFos+ cells only reflect a subset of an engram that is otherwise distributed throughout the brain and recruits numerous immediate early genes, cell types, and complementary physiological activity that activity-dependent markers may fail to capture due to the relatively slow timescales of gene expression. We indeed note that while cFos+ cells indicate recent neural activity, a cell that was recently active does not necessarily have to express cFos especially across brain regions and cell types which presumably have their own thresholds for cFos expression. These points highlight the complex nature of a memory engram and underscore a caution that is warranted when

interpreting data in light of inherent technical limitations. We believe that a multi-faceted approach combining genetic tagging strategies with real-time imaging during complex behaviors will help to disentangle the relationship between neural activity, genetic modifications, and systems-level changes in response to learning and memory.

Our terminal manipulations are in line with recent studies demonstrating terminal-specific routing of information from vCA1 cell bodies through a variety of single, bi-, and trifurcating processes[8,41,42]. Our data provide a "gain-of-function" demonstration that activated vCA1 terminals can drive preference or aversion, which we believe was obfuscated by cell body stimulation given that the latter presumably activates the cell body and most, if not all, corresponding axonal outputs. The former would selectively modulate a set of terminals emerging from vCA1 that project to a distinct target area while only minimally affecting vCA1 terminals projecting to other target areas. Additionally, while the molecular basis underlying our valence "switch" experiments remain unknown, we posit that the plasticity of the transcriptome could confer the ability to the switch which aspect of behavior a terminal drives given the rapid and enduring responses to learning and memory present at the genetic level in tagged cells.[43] Indeed, the comprehensive transcriptional landscape in the mouse hippocampus is dynamic across the lifespan of memory formation and recall, and its experience-dependent modifications are largely present specifically in tagged cells within minutes of learning and lasting for several weeks[42]. Future experiments may perform RNA-seq on cells before and after the induction protocol to measure the ensuing transcriptional changes and identify putative loci mediating such functional plasticity.

Finally, while the physiological basis by which terminals can switch or reset their capacity to drive valence-specific behaviors remains unclear, future studies may consider candidate mechanisms including homeostatic plasticity, dendritic growth and retraction, and counter-conditioning-facilitated changes along the axon-dendrite interface between vCA1 and the BLA or NAc[25, 26]. In line with this speculation, previous studies have demonstrated that the dorsal hippocampus contains defined sets of functionally plastic cell bodies sufficient to drive fear or reward, while the BLA contains fixed populations that are sufficient to drive each behavior contingent on the anatomical location stimulated along the anterior-posterior axis as well as on their projection-specific sites.[7,8,25-27] Subsequent research can be aimed at utilizing our dual-memory tagging approach to genetically and physiologically map out which cell-types and circuits show such hardwired or experience-dependent responses to emotional memories as well. In our study, we believe that vCA1 cells become positive or negative in an experience-dependent manner as opposed to being hardwired for either valence per se, as has been observed in many other brain regions (e.g. BLA[25]). However, though it remains possible that a subset of these vCA1 cells are preferentially tuned to process a given valence in an experience-independent manner. Indeed, the notion that experience itself modifies these neurons to become positive or negative does not preclude the possibility that subsequent experiences will modify their capacity in a flexible manner to drive a given behavior associated with a given valence.

Together, we propose that, in addition to processing spatio-temporal units of information, the hippocampus contains discrete sets of cells processing fear and reward that relay content-specific

and behaviorally-relevant information to downstream areas in a molecularly-defined and projection-specific manner, thus collectively providing a multi-synaptic biological substrate for multiple memory engrams.

ONLINE METHODS

Subjects. Fos^{CreER} (Jax stock: #021882) and Wildtype male C57BL/6 mice (2-3 months of age; Charles River Labs) were housed in groups of 5 mice per cage. The animal vivarium was maintained on a 12:12-hour light cycle (lights on at 0700). Mice were placed on a diet containing 40 mg/kg doxycycline (Dox) for a minimum of 48 hours prior to surgery with access to food (doxycycline diet) and water *ad libitum*. Mice were given a minimum of ten days after surgery to recover. Dox-containing diet was replaced with standard mouse chow (*ad libitum*) 48 hours prior to behavioral tagging to open a time window of activity-dependent labeling[1,2]. All subjects were treated in accordance with protocol 17-008 approved by the Institutional Animal Care and Use Committee at Boston University.

Stereotaxic Surgery and Optic Implant. Stereotaxic injections and optical fiber implants follow methods previously reported.[1,2] All surgeries were performed under stereotaxic guidance and subsequent coordinates are given relative to bregma (in mm) dorsal ventral injections were

calculated and zeroed out relative to the skull. Mice were placed into a stereotaxic frame (Kopf Instruments, Tujunga, CA, USA) and anesthetized with 3% isoflurane during induction and lowered to 1-2% to maintain anesthesia (oxygen L/min) throughout the surgery. Ophthalmic ointment was applied to both eyes to prevent corneal desiccation. Hair was removed with a hair removal cream and the surgical site was cleaned three times with ethanol and betadine. Following this, an incision was made to expose the skull. Bilateral craniotomies involved drilling windows through the skull above the injection sites using a 0.5 mm diameter drill bit. Coordinates were -3.16 anteroposterior (AP), ±3.1 mediolateral (ML), and -4.6 dorsoventral (DV) for vCA1; -1.8 AP, ± 3.1 ML, and -4.7 DV for the BLA; -1.25 AP, ± 1.0 ML, and -4.7 DV for the NAc; 1.70 AP, ± 0.35 ML, and -2.8 DV for the PFC. All mice were injected with a volume of 300nl of cocktail per site at a control rate of 100 µl min^{-1} using a mineral oil-filled 33-gage beveled needle attached to a 10 µl Hamilton microsyringe (701LT; Hamilton) in a microsyringe pump (UMP3; WPI). The needle remained at the target site for five minutes post-injection before removal. For all targets, bilateral optic fibers were placed 0.5 DV above the injection site. Jewelry screws secured to the skull acted as anchors. Layers of adhesive cement (C&B Metabond) followed by dental cement (A-M Systems) were spread over the surgical site. Mice received 0.1 mL of 0.3 mg/ml buprenorphine (intraperitoneally) following surgery and were placed on a heating pad during surgery and recovery. Histological assessment verified viral targeting and fiber placements. Data from off-target injections were not included in analyses.

Activity-dependent Viral Constructs. pAAV9-cFos-tTA, pAAV9-TRE-eYFP and pAAV9-TRE-mCherry were constructed as previously described (Ramirez et al., 2015). AAV9-c-Fos-tTA was combined with AAV9-TRE-eYFP or AAV9-TRE-ChR2-EYFP (UMass Vector core) prior to

injection at a 1:1 ratio. This cocktail was further combined in a 1:1 ratio AAV9-CAG-Flex-DIO-TdTomato (UNC Vector Core).

Optogenetic Methods. Optic fiber implants were plugged into a patch cord connected to a 450nm laser diode controlled by automated software (Doric Lenses). Laser output was tested at the beginning of every experiment to ensure that at least 15 mW of power was delivered at the end of the patch cord (Doric lenses).

Behavior Tagging. When animals were off Dox, as previously reported[9-12], Dox diet was replaced with standard lab chow (*ad libitum*) 48-hours prior to behavioral tagging. Female exposure: One female mouse (PD 30-40) was placed into a clean home cage with a clear cage top. The experimental male mouse was then placed into the chamber and allowed to interact freely for 2 hours. Fear exposure: Mice were placed into a conditioning chamber and received four 1.50mA (2s) foot shocks over an 8-minute training session. Following tagging, Dox was reintroduced to the diet and the male mice were returned to their home cage with access to Dox diet. For 4-OHT tagging, 4-hydroxytamoxifen (Sigma: H7904) was diluted into 100% ethanol and vortexed for 5 minutes. Once in solution, corn oil was added and the solution was sonicated to achieve a dilution of 10mg/kg stock. When the solution was ready, 4-OHT was loaded into syringes for injection and any left-over solution was placed in the -20C to be used in the future. On the day of tagging, 200mg of 10mg/ml stock (2mg 4OHT) was administered I.P. in Fos^{creER} mice 30 minutes following behavior and were left undisturbed for 72 hours. Mice were injected with saline or DMSO at least twice prior to tagging protocol to acclimate animals to injection and prevent off target tagging.

Behavioral Assays. All behavior assays were conducted during the light cycle of the day (0700–1900). Mice were handled for 3–5 days, 5-10 minutes per day, before all behavioral experiments. The testing chamber consisted of a custom-built rectangular box with a fiber optic holder (38 x 23.5 x 42 cm). Red tape divided the chamber down the middle, creating two halves. Right and left sides for stimulation were randomized. Day 1 was used to assess baseline levels, during which the mouse was given 10 minutes to freely explore the arena. Animals were rerun in baseline days if they showed more than a 45-55% preference for either side. Animals were acclimated to the chamber until they had a minimum of a 45/55 preference. Once baseline is achieved, the day following the first engram tag, mice received light stimulation (15 ms pulses at 20-Hz) upon entry in the designated side of the chamber (counterbalanced across groups) over a 10-minute test period. Once the mouse entered the stimulated side, a TTL signal from the EthoVision software via a Noldus USB-IO Box triggered a stimulus generator (STG-4008, Multi-channel Systems). 6A video camera (Activeon CX LCD Action Camera) recorded each session and an experimenter blind to treatment conditions scored the amount of time on each side. Statistical analyses involved one-way ANOVAs comparing group difference scores [time (in seconds) on stimulated side minus time on unstimulated side] as well as changes across days using matching or repeated measures one-way ANOVA. Behavioral diagrams were made with BioRender.

Optogenetic Induction Protocol. For optogenetic **fear induction**, subjects were placed in a shock chamber with light stimulation (20 Hz, 15ms) for 500 seconds. Foot shocks (1.5 mA, 2s duration) were administered at the 198s, 278s, 358s, and 438s time points. During optogenetic **reward induction**, in a different room from the initial fear tag, the subject was placed into a clean homecage with a female mouse. Light stimulation (20Hz, 15ms) was applied to the male mouse for 10 minutes.

Immunohistochemistry. Immunohistochemistry follows protocols previously reported[15, 16, 18]. Mice were overdosed with 3% isoflurane and perfused transcardially with cold (4° C) phosphate-buffered saline (PBS) followed by 4% paraformaldehyde (PFA) in PBS. Brains were extracted and stored overnight in PFA at 4°C. Fifty µm coronal sections were collected in serial order using a vibratome and collected in cold PBS. Sections were blocked for 1 hour at room temperature in PBST and 5% normal goat serum (NGS) or Bovine albumin serum (BSA) on a shaker. Sections were transferred to wells containing primary antibodies (1:1000 guinea anti-c-Fos [SySy]; 1:1000 rabbit anti-RFP [Rockland]; 1:5000 chicken anti-GFP [Invitrogen]) and allowed to incubate on a shaker overnight at room temperature or 3 days at 4 degrees C. Sections were then washed in PBST for 10-min (x3), followed by 2-hour incubation with secondary antibody (1:200 Alexa 555 anti-rabbit [Invitrogen]; 1:200 Alexa anti-guinea 647 [Invitrogen]; 1:200 Alexa 488 anti-chicken [Invitrogen]). Following three additional 10-min washes in PBST, sections were mounted onto micro slides (VWR International, LLC). Vectashield Hart Set Mounting Medium with DAPI (Vector Laboratories, Inc) was applied, slides were cover slipped, and allowed to dry overnight.

Cell Quantification. Only animals that had accurate bilateral injections were selected for quantification. Fluorescent images were acquired using a confocal microscope (Zeiss LSM800, Germany) at the 20X objective. For cfos quantification, all animals were sacrificed 90 minutes post-behavior for immunohistochemical analyses. The number of EYFP, TdTomato, and *c-Fos*-immunoreactive neurons in the vCA1 were counted to measure the number of active cells in the respective area. 3– 5 coronal slices (spaced 50 um from each other) per mouse of which the means were taken; each N value contains 3-5 image quantification for 3-5 mice. The number of eYFP-positive, TdTomato-positive, and *c-Fos*-positive, and DAPI-positive cells in a set region of interest

(ROI) were quantified manually across two different experimenters with ImageJ (https://imagej.nih.gov/ij/). The size of the ROI was standardized across brains, animals, experiments, and groups. The two counters were blind to experimental and control groups. To calculate the percentage of tagged cells we counted the number of fluorescently positive cells and divided them by the total number of DAPI cells. Overlaps were counted as a percentage over DAPI as well, for example, cells that were positive for both EYFP and TdTomato were counted over DAPI. Venn Diagram charts are representative graphs of the proportion of EYFP+, TdTomato+, and cfos+ cells normalized to 100% not to DAPI.

Fluorescence Intensity Calculations

50 micron coronal sections were stained with chicken anti GFP (1:1000) and rabbit anti RFP (1:1000) as described above. Fluorescent images were taken at 20X magnification using a confocal microscope (Zeiss LSM800, Germany). All laser and imaging settings were maintain consistent across all animals and all brain regions imaged. Regions of interest (ROIs) were maintained consistent across images, sections, and animals. ROIs were identified using landmarks and referencing the Paxinos & Franklin Mouse Brain Atlas. Fluorescence quantification was conducted in ImageJ. After manual selection of the ROI using the selections tool, we set to gather information for area integrated density and mean grey value. Images were analyzed for EYFP and TdTomato separately. Within each image we gathered information about the average fluorescence of the terminals as well as background/baseline levels of a negative region to have a means of normalization. From here we used the following formula for Corrected Total Fluorescence (CTF) = integrated density – (area of selected ROI X mean fluorescence of baseline/background readings).[44,45,46] This gave us the arbitrary units for average fluorescence intensity of our EYFP vs TdTomato terminals of interest.

Image Integrity. Acquired image files (.czi) were opened in ImageJ. Processing of images in Figure 1 involved maximizing intensity, removing outlier noise, and adjusting contrast of images.

Data Analysis. Data were analyzed using Prism (GraphPad Software, La Jolla, CA) and Statistica 13 data analysis software (TIBCO Software, Inc., Palo Alto, CA). Data were analyzed using paired t-tests (two factors), unpaired t-tests, one-way or two-way ANOVAs with repeated measures ANOVAs (more than two factors), where appropriate. Post-hoc analyses(Tukey's multiple comparisons test) were used to characterize treatment and interaction effects, when statistically significant alpha set at $p < 0.05$, two-tailed). Statistical analyses are reported in figure captions.

Generation of Single Cell Suspension from Mouse Hippocampal Tissue. Five-week old male mice labeled with ChR2-YFP transgene[1] after conditioning were euthanized by isoflurane. Mouse brains were rapidly extracted, and the hippocampal regions were isolated by microdissection. Eight mice were pooled by each experimental condition. Single cell suspension was prepared according to the guideline of Adult Brain Dissociation Kit (Miltenyi Botec, Cat No: 13-107-677). Briefly, the hippocampal samples were incubated with digestion enzymes in the C Tube placed on the gentleMACS Octo Dissociator with Heaters with gentleMACS Program: 37C_ABDK_01. After termination of the program, the samples were applied through a MACS SmartStrainer (70 µm). Then a debris removal step and a red blood cell removal step were applied to obtain single cell suspension.

Isolation of YFP-positive single cell by FACS. The single cell suspension was subject to a BD FACSAria cell sorter according to the manufacturer's protocol to isolate EYFP-single cell population.

Preparation of RNA-seq library. The RNA of FACS isolated YFP-positive cells was extracted by using Trizol (Life Technologies) followed by Direct-zol kit (Zymo Research) according to manufacturer's instructions. Then the RNA-seq library was prepared using SMART-Seq® v4 Ultra® Low Input RNA Kit (TaKaRa).

Analysis of RNA-seq data. The resulting reads from Illumina had good quality by checking with FastQC (http://www.bioinformatics.babraham.ac.uk/projects/fastqc/). The first 40 bp of the reads were mapped to mouse genome (mm10) using STAR[29], which was indexed with Ensembl GRCm38.91 gene annotation. The read counts were obtained using featureCounts[30] function from Subread package with unstranded option. Reads were normalized by library size and differential expression analysis based on negative binomial distribution was done with DESeq2[52]. Genes with FDR-adjusted p-value less than 0.00001 plus more than 4-fold difference were considered to be differentially expressed. Raw data along with gene expression levels are being deposited to NCBI Gene Expression Omnibus. For Gene Ontology analysis, we ranked protein-coding genes by their fold changes and used as the input for GseaPreranked tool[53]. Based on the GSEA outputs, the dot plots were created with a custom R script. The pathways with FDR- adjusted p-value less than 0.25 were considered to be enriched.

Sampling strategy. Subjects were randomly assigned to groups. No statistical methods were used to determine sample size; the number of subjects per group were based on those in previously published studies and are reported in figure captions.

Reproducibility. Behavioral experiments were replicated at least three times with three different experimenters. The first experiments were run at a different institution and the last two replications were run at Boston University. Not only did the behavioral findings stand across experimenters (1 male, 2 females), but it stood across institutions as well. Sequencing data was replicated twice as well to confirm original findings. All behavioral and cell counters and scorers were blinded to experimental and control groups.

Slice electrophysiology recording. FosCRE-ERT2 male mice were injected with a 1:1 ratio of AAV-CAG-FLEX-TdTomato + AAV-cfos-tTA+AAv-TRE-EYFP into the ventral hippocampus. Animals were counterbalanced for the experiment where half received positive tagging with 4OHT and negative tagging with Dox and the other half received negative tagging with 4OHT and positive tagging with Dox. Coronal slices of the ventral hippocampus were prepared from previously injected animals, 3-5 days post tagging experience. Animals were deeply anesthetized with isoflurane anesthesia, decapitated and the brains were removed. Brain slices were prepared in oxygen perfused sucrose-substitute artificial cerebrospinal fluid (ACSF). Solution contained: 185 mM NaCl, 2.5 mM KCl, 1.25 mM NaH_2PO_4, mM $MgCl_2$, 25 mM $NaHCO_3$, 12.5 mM glucose, and 0.5 mM $CaCl_2$. 400 µm slices were cut via Leica VT 1200 (Leica Microsystems) and incubated in 30°C ACSF consisting of 125 mM NaCl, 25 mM $NaHCO_3$, 25 mM D-glucose, 2 mM KCl, 2 mM $CaCl_2$, 1.25 mM NaH_2PO_4, and 1 mM $MgCl_2$, for 20 minutes and then cooled to room-temperature. Two-photon imaging system (Thorlabs Inc.) was used to distinguish positive and

negative cells. Imaging system is equipped with a mode-locked Ti:Sapphire laser (Chameleon Ultra II; Coherent) which was set to wavelengths between 920 nm to 950 nm in order to excite Alexa Fluor 488 and 568, tdTomato and EYFP fluorophores using a 20x , NA 1.0 objective lens (Olympus). In order to ensure differences between the two populations is not attributable to the type of virus used for tagging the neurons, two groups of animals were prepared. In one group positive memories tagged with tdTomato and negative ones with EYFP and in the other one vice versa. Patch-clamp electrodes with 0.6–1 μm tips were pulled via horizontal puller (Sutter Instruments), and pipette resistance was recorded between 4 and 6 MΩ. Pipettes were filled with intracellular fluid containing: 120 mM K-gluconate, 20 mM KCl, 10 mM HEPES, 7 mM diTrisPhCr, 4 mM Na_2ATP, 2 mM $MgCl_2$, 0.3 mM Tris-GTP, and 0.2 mM EGTA; buffered to pH 7.3 with KOH. 0.15% weight/volume of Alexa Fluor (Thermo Fisher Scientific) 488 hydrazide (for recording from tdTomato cells) or 567 (for recording from EYFP cells) were added to visualize the recording pipette under the imaging system. Prior to breaking into the cells, pipette capacitance neutralization and bridge balance compensation were performed . Data was acquired using Multiclamp 700B (Molecular Devices) and a Digidata 1550 (Molecular Devices) with sampling rate of 10kHz.

Electrophysiology data analysis. Brain slice electrophysiology data analysis was performed in python with custom written scripts using pyABF package (http://swharden.com/pyabf/). For spike shape analysis , spike onsets were identified using their first derivative, corresponding voltage was called spike onset. Spike half-width indicates the time between the two halves of peak voltage. For dynamic analysis of spiking properties stepwise current injections were performed. Firing threshold is the voltage at which a neuron fires at least a single spike, and firing onset is the corresponding current. FI gain was calculated as change in the firing frequency from the lowest to

the highest frequency of firing divided by current injected. Adaptation ratio was obtained by dividing the mean inter spike intervals (ISIs) during the last 200 ms of spiking by the mean ISIs during the first 200 ms of spiking. Comparison between positive and negative memory cells were done both within a single slice, within an animal as well as across animals to control for potential differences between animals or slices. Since the results in all three situations were similar, the pooled data for comparison of different groups d'Agostino-Pearson K2 test was used to determine normality of data. Based on the normality results, either independent t-test (normal distribution) or Mann-Whitney-Wilcoxon test two-sided with Bonferroni correction were used.

Figure Descriptions

Figure 1 | Hippocampus cells processing positive or negative memory engrams are preferentially reactivated by their respective valences

a, Fos-CreERT2 mice were injected with a viral cocktail of 1:1 ratio of AAV9-c-Fos-tTA and AAV9-TRE-EYFP mixed in at 1:1 with AAV-Flex-DIO-TdTomato into the vHPC to create the ability to open two windows of tagging in the mouse. **b,** Schematic of the timeline for TAG1 and TAG2 which are doxycycline and 4-hydroxytamoxifen dependent, respectively. The negative tag consists of 4 foot shocks and the positive tag consists of male to female exposure. **c,** Representative image of dual memory segregation in a sagittal section of the vHPC, specifically vCA1. **d,** Quantification (%Labeling) of EYFP+ (Negative) and TdTomato+ (Positive) cells over DAPI along the anterior-posterior axis of vCA1 showing the segregation of valence. (N=3) **e,** Schematic to visualize cells active during three different behavioral experiences. TAG1 is doxycycline dependent in EYFP, TAG2 is 4-OHT dependent in TdTomato, and lastly, Experience3 is

visualized with immunohistochemistry by staining for endogenous cfos 90 minutes after a behavioral experience. **f,** Schematic of groups for visualizing triple memory overlaps (n=4-6 per group). Groups were counterbalanced to avoid potential timeline biases **g,** Representative images of triple memory overlaps in vCA1 with a 20x zoom in showing the different representative overlaps. **h**, The number of tagged neurons in vCA1 are similar between EYFP, TdTomato, and cfos; there is no statistical difference between recruitment. (Multiple comparisons one-way Anova; N=10-12) **i,** Percent overlap for respective behavioral tags for EYFP + Tdtomato for Negative + Positive (N+P; Group 1), Negative + Negative (N+N; Group 2), Positive + Negative (P+N; Group 3), and Positive + Positive (P+P; Group4), ($F(3, 12) = 170.0$, $P<0.0001$). j, overlap counts for EYFP + TdTomato + cfos ($F(3, 12) = 10.55$, $P=0.0011$).

Figure 2 | Ventral hippocampal neurons encoding positive or negative valences have discrete projection patterns. a, Fos-CreERT2 mice were injected with a viral cocktail of 1:1 ratio of AAV9-c-Fos-tTA and AAV9-TRE-EYFP mixed in with AAV-Flex-DIO-TdTomato into the vHPC for dual memory tagging. **b,** Experimental timeline for tagging; EYFP represents Negative and TdTomato represents positive. **c-d,** Representative images of terminal projections; anterior, medial, and posterior BLA, dorsal hippocampus, prefrontal cortex, nucleus accumbens, dorsal medial hypothalamic nucleus, and the fornix. **e-f,** Quantification of fluorescence with arbitrary units of both EYFP and TdTomato across the different brain regions from the representative images (N=3)

Figure 3 | Distinct molecular landscapes of positive and negative hippocampus engram cells

a, Experimental scheme to label, isolate, and analyze the two groups of vCA1 cells labeled by EYFP upon negative stimulation (electrical shock) or positive stimulation (male mice engaged in

social interaction with female mice) or neutral conditioning in the same cage without negative or positive stimulation. **b.** FACS isolation of EYFP-positive nuclei from the hippocampi of mice labeled by AAV9-cFos-tTA + AAV9-TRE-ChR2-EYFP virus from their respective groups **c**, Percentage of EYFP-positive nuclei from each group. **d**, A Volcano plot with the relative fold change of gene expression in log 2 ratio and the FDR-adjusted p-value in log 2 ratio as X and Y axis showing the up and down regulated genes in negative vCA1 cells compared to neutral group. Up or down regulated genes with FDR adjusted p-value less than 1e-5 plus at least four-fold differences were highlighted in either red or blue respectively. The gene names were displayed for the top 20 most significant genes as sorted by Wald statistics. **e**, A Volcano plot showing the up and down regulated genes in positive vCA1 cells compared to neutral group. **f**, A Venn diagram showing the 1,104 differentially expressed genes (DEGs) in positive and 474 DEGs in negative vCA1 cells. 262 DEGs were identified in both groups. **g**, An UpSet plot showing 226 down regulated genes in both negative and positive vCA1 cells, and 35 up regulated genes in both negative and positive vCA1 cells. Only one gene (*Nufip1*) was upregulated in positive engram but down regulated in negative engram. **h**, Gene Enrichment Set Analysis of the up regulated pathways in negative engrams using Gene Ontology (GO) module. The size of the dot represents the gene count and the color of the dot indicates the FDR. The pathway with an FDR-adjusted P value smaller than 0.25 is considered as significantly enriched. **i**, GO analysis of down regulated pathways in negative vCA1 cells. **j**, GO analysis of up regulated pathways in positive vCA1 cells. **k**, GO analysis of down regulated pathways in positive vCA1 cells.

Figure 4 | Hippocampal valence specific outputs are sufficient to drive preference or aversion in a projection-specific and functionally reversible manner

Mice were injected with a virus cocktail of AAV9-c-Fos-tTA AAV9-TRE-ChR2-EYFP or AAV9-TRE-EYFP into vCA1 and optic fibers were placed bilaterally over the cell bodies of vCA1 or the terminals from vCA1 to the BLA, Nac, or the PFC, in separate groups. The mice were then tagged with either a negative or positive experience and subjected to real time opto-place avoidance and preference. **a**, Representative images of ChR2-EYFP labeling cell bodies in vCA1 and its respective terminals in the BLA, NAc, and PFC. **b**, Fear to reward protocol in which the subjects received stimulation of vCA1 cell body or vCA1 projections to the BLA, NAc, or PFC terminals. **d**, Percent preference for the stimulation side at baseline, pre-induction, and post-induction (n = 7 subjects for EYFP controls, n=8 subjects for vCA1, n = 8 subjects for BLA, n = 7 for NAc, and n = 7 for PFC, **P = 0.0018, ***P = 0.0006, repeated measures one-way ANOVA followed by Tukey's multiple comparison test). **e**, Reward to Fear protocol in which the subjects received stimulation of BLA, NAc, or PFC terminals originating from vCA1. **f**, Percent preference for the stimulation side at baseline, pre-induction, and post-induction (n = 7 for EYFP, n=9 for vCA1, n = 8 for BLA, n = 7 for NAc, and n = 7 for PFC, **P = 0.0032, ****P < 0.0001, repeated measures one-way ANOVA followed by Tukey's multiple comparison test).

Acknowledgements.

We thank Dr. Joshua Sanes and his lab at the Center for Brain Science, Harvard University, for providing laboratory space within which the initial experiments were conducted, especially the early members of the lab, Emily Merfeld, Emily Doucette, Stephanie Grella, and Joseph Zaki. Further we thank the Center for Brain Science Neuroengineering core for providing technical support, and the Society of Fellows at Harvard University for their support. This work was supported by an NIH Early Independence Award (DP5 OD023106-01), an NIH Transformative R01 Award, a Young Investigator Grant from the Brain and Behavior Research Foundation, a

Ludwig Family Foundation grant, the McKnight Foundation Memory and Cognitive Disorders award, and the Center for Systems Neuroscience and Neurophotonics Center at Boston University.

Author Contributions

M.S. and O.M. conducted and analyzed histology. M.S., O.M., and E.R. ran and analyzed optogenetic experiments. B.Y. and X.S.L. performed RNA-seq and corresponding analyses. B.R. and F.R.F. conducted in vitro physiological experiments and analyses. M.S., O.M., X.S.L. and S.R. designed the project. M.S. X.S.L. and S.R. wrote the manuscript. All authors edited and commented on the manuscript.

Declaration of Interests

The authors declare no competing interests.

References

1. Gergues, M.M., et al. Circuit and molecular architecture of a ventral hippocampal network. *Nature neuroscience*, *23*(11), 1444–1452 (2020)
2. Josselyn, S.A. & Tonegawa, S. Memory engrams: Recalling the past and imagining the future. *Science* **367**(6473) (2020)
3. Josselyn, S., Köhler, S. & Frankland, P. Finding the engram. *Nat Rev Neurosci* **16,** 521–534 (2015)
4. Cai, D. J., et al. A shared neural ensemble links distinct contextual memories encoded close in time, *Nature* **000**, 1-4 (2016).
5. M. S. Fanselow, M. S. & Dong, H.W., Neuron 65, 7–19 (2010).

6. Gaurgier J. L. & Tank, D. W. A dedication population for reward coding in the hippocampus, *Neuron* **99**, 179-193 (2018).
7. Xu, C. et al. Distinct hippocampal pathways mediate dissociable roles of context in memory retrieval, *Cell* **167**, 1-2 (2016).
8. Ciocchi, S., Passecker, J., Malagon-Vina, H., Mikus, N., & Klausberger, T. Selective information routing by ventral hippocampal CA1 projection neurons, *Science* 348, 560-563 (2015).
9. Padilla-Coreano, N. et al. Direct Ventral Hippocampal-Prefrontal Input is Required for Anxiety-Related Neural Activity and Behavior, *Neuron* **89**, 857-866 (2016).
10. Kim, J., Pignatelli, M., Xu, S., Itohara, S. & Tonegawa, S. Antagonistic negative and positive neurons of the basolateral amygdala. *Nat. Neurosci.* **19**, 1636–1646 (2016).
11. Liu, X. et al. Optogenetic stimulation of a hippocampal engram activates fear memory recall. *Nature* **484**, 381–385 (2012).
12. Ramirez, S. et al. Creating a false memory in the hippocampus. *Science* **341**, 387–391 (2013).
13. Redondo, R. L. et al. Bidirectional switch of the valence associated with a hippocampal contextual memory engram. *Nature* **513**, 426–430 (2014).
14. Ryan, T. J., Roy, D. S., Pignatelli, M., Arons, A. & Tonegawa, S. Engram cells retain memory under retrograde amnesia. *Science* **348**, 1007–1013 (2015).
15. Gore, F. et al. Neural representations of unconditioned stimuli inn basolateral amygdala mediate innate and learned responses. *Cell***162,** 134-145 (2015).
16. Rashid, A. J. et al. Competition between engrams influences fear memory formation and recall, *Science* **353**, 383-38 (2017).

17. Yokose, J. et al. Overlapping memory trace indispensable for linking, but not recalling, individual memories, *Science* **355**, 398-403 (2017).

18. DeNardo, L. A. et al. Temporal evolution of cortical ensembles promoting remote memory retrieval. *Nature Neuroscience* ***22*(3)**, 460–469. (2019).

19. Ramirez, S., Liu, X., MacDonald, C. *et al.* Activating positive memory engrams suppresses depression-like behaviour. *Nature* **522,** 335–339 (2015).

20. Chen, B. K., Murawski, N. J., et al Artificially enhancing and suppressing hippocampus-mediated memories. *Current Biology*, **29(11)**, 1885-1894.e4 (2019)

21. Rodriguez, E. et al. Identifying Parabrachial neurons selectively regulating satiety for highly palatable food in mice. *Eneuro* **6(6)**, ENEURo.0252-19 .(2019)

22. Peters, J., Dieppa-Perea,L. M., Melendez, L. M., & Quirk, G. J. Induction of fear extinction with hippocampal-infralimbic BDNF, *Science* **328**, 1288-1290 (2010).

23. Gan, L., Cookson, M.R., Petrucelli, L. *et al.* Converging pathways in neurodegeneration, from genetics to mechanisms. *Nat Neurosci* **21,** 1300–1309 (2018).

24. Warden, M.R. et al. A prefrontal cortex-brainstem neuronal projection that controls response to behavioural challenge, *Nature* **428**428-432 (2012).

25. Beyeler, A. et al. Divergent Routing of Positive and Negative Information from the Amygdala during Memory Retrieval, *Neuron* **90,**348-361 (2016).

26. Namburi, P. et al. A circuit mechanism for differentiating positive and negative associations, *Nature* **520**, 675-678 (2015).

27. Jimenez, J. C. et al. Anxiety cells in a hippocampal-hypothalamic circuit. *Neuron* **97**. 1-14 (2018).

28. Spellman, T., Rigotti, M., Ahmari, S. *et al.* Hippocampal–prefrontal input supports spatial encoding in working memory. *Nature* **522,** 309–314 (2015).

29. Xiu, J., Zhang, Q., Zhou, T. *et al.* Visualizing an emotional valence map in the limbic forebrain by TAI-FISH. *Nat Neurosci* **17,** 1552–1559 (2014).

30. Dobin, A, et al. STAR: ultrafast universal RNA-seq aligner, *Bioinformatics* **29**, 15-21 (2013).

31. Liao,Y., Smyth, G.K., & Shi, W. featureCounts: an efficient general purpose program for assigning sequence reads to genomic features, *Bioinformatics* **30**, 923-930 (2014).

32. Knapska, E., Mikosz, M., Werka, T., & Maren, S. Social modulation of learning in rats. *Learning & memory (Cold Spring Harbor, N.Y.)*, *17*(1), 35–42. (2009).

33. Nakazawa, Yuki, et al. "Memory Retrieval along the Proximodistal Axis of CA1." *Hippocampus* 9, 1140–48.

34. Zhou, Y., et al,. A ventral CA1 to nucleus accumbens core engram circuit mediates conditioned place preference for cocaine. *Nature neuroscience*, *22*(12), 1986–1999. (2019)

35. Graham, Kourtney, et al. "Hippocampal and Thalamic Afferents Form Distinct Synaptic Microcircuits in the Mouse Infralimbic Frontal Cortex." *Cell Reports* 3, p. 109837. (2021)

36. Ye, Li, et al. "Wiring and Molecular Features of Prefrontal Ensembles Representing Distinct Experiences." *Cell* 7, 1776–88. (2016)

37. Goode, Travis D., et al. "An Integrated Index: Engrams, Place Cells, and Hippocampal Memory." *Neuron* 5, 805–20. (2020)

38. Rao-Ruiz, Priyanka, et al. "Engram-Specific Transcriptome Profiling of Contextual Memory Consolidation." *Nature Communications* 1. (2019)

39. Reijmers, Leon. "Genetic Control of Active Neural Circuits." *Frontiers in Molecular Neuroscience* (2009)

40. Sweis, Brian M., et al. “Dynamic and Heterogeneous Neural Ensembles Contribute to a Memory Engram.” *Current Opinion in Neurobiology* 199–206 (2021)

41. Arszovszki, Antonia, et al. “Three Axonal Projection Routes of Individual Pyramidal Cells in the Ventral CA1 Hippocampus.” *Frontiers in Neuroanatomy* (2014)

42. Chen, Michelle B., et al. “Persistent Transcriptional Programmes Are Associated with Remote Memory.” *Nature* 7834, 437–42. *(2020)*

43. Marco, Asaf, et al. “Mapping the Epigenomic and Transcriptomic Interplay during Memory Formation and Recall in the Hippocampal Engram Ensemble.” *Nature Neuroscience* 12, 1606–17 (2020)

44. Donohue, Jordan D., et al. “Parahippocampal Latrophilin-2 (ADGRL2) Expression Controls Topographical Presubiculum to Entorhinal Cortex Circuit Connectivity.” *Cell Reports* 8-110031. (2021)

45. Phillips, Mary L., et al. “Ventral Hippocampal Projections to the Medial Prefrontal Cortex Regulate Social Memory.” *ELife* (2019)

46. Shihan, Mahbubul H., et al. “A Simple Method for Quantitating Confocal Fluorescent Images.” *Biochemistry and Biophysics Reports* 100916. (2021)

47. Bardoni, B., Schenck, A., and Mandel, J.L.. A novel RNA-binding nuclear protein that interacts with the fragile X mental retardation (FMR1) protein. Hum Mol Genet *8*, 2557-2566 (1999)

48. Duke, C.G., Kennedy, A.J., Gavin, C.F., Day, J.J., and Sweatt, J.D. Experience-dependent epigenomic reorganization in the hippocampus. Learning & memory *24*, 278-288 (2017).

49. Hagerman, R.J., Berry-Kravis, E., Hazlett, H.C., Bailey, D.B., Jr., Moine, H., Kooy, R.F., Tassone, F., Gantois, I., Sonenberg, N., Mandel, J.L.*, et al.* Fragile X syndrome. Nat Rev Dis Primers *3*, 17065 (2017)

50. Halder, R., Hennion, M., Vidal, R.O., Shomroni, O., Rahman, R.U., Rajput, A., Centeno, T.P., van Bebber, F., Capece, V., Garcia Vizcaino, J.C.*, et al.* DNA methylation changes in plasticity genes accompany the formation and maintenance of memory. Nat Neurosci *19*, 102-110 (2016)

51. Sidorov, M.S., Auerbach, B.D., and Bear, M.F. Fragile X mental retardation protein and synaptic plasticity. Molecular brain *6*, 15 (2013)

52. Love, Michael I., et al. "Moderated Estimation of Fold Change and Dispersion for RNA-Seq Data with DESeq2." *Genome Biology*, no. 12. (2014)

53. Subramanian, A., et al. "Gene Set Enrichment Analysis: A Knowledge-Based Approach for Interpreting Genome-Wide Expression Profiles." *Proceedings of the National Academy of Sciences*, no. 43, pp. 15545–50 (2005)

Extended Data Figures

Extended Data Fig 1: Representative image of TRAP2 'leakiness' in vHPC. a Representative image of TdTomato expression in mouse with DMSO injection instead of 4-OHT. **b** EYFP expression in the same mouse while remaining on DOX continuously. **c** DAPI.

Extended Data Fig 2: Cell recruitment based on valence type and cfos overlap measures. a No significant (ns) difference in % overlap of EYFP over DAPI for shock vs female tags. **b** % No significant (ns) difference in % overlap of TdTomato over DAPI for shock vs female tags. **c** No significant (ns) difference in % overlap of cfos over DAPI for shock vs female tags. **d** NS difference in cfos+EYFP overlapping cells in restraint stress + shock vs. sweetened condensed milk + female exposure. **e** similar valences shock and stress and female and milk highly overlap with one another when compared to overlap of different valences, female and stress and shock and milk. Multiple comparisons one-way ANOVA; $F(3, 12) = 20.77$, $P<0.0001$.

Extended Data Fig 3: Repreparation of total tagged cells and their overlaps. GROUP1, 2, 3, & 4 here are the same group orders as shown in Figure 1. GROUP 1: Shock (Negative) + Female (positive) + Stress (restraint stress); GROUP 2: Shock + Shock + Stress; GROUP 3: Female + Shock + Milk; GROUP 4: Female + Female + Milk. a-d, representative venn diagrams portraying valenced overlaps as a total population of tagged cell. Normalized to 100%.

Extended Data Fig 4: **Negative and positive valenced cells in the ventral hippocampus share similar electrophysiological characteristics. a** Fos-CreERT2 were injected with a virus cocktail of AAV-Flex-DIO-TdTomato, AAV9-c-Fos-tTA and AAV9-TRE-EYFP to tag either negative or positive experiences within the same animal for slice electrophysiology. **b** Representative image of cells processing a negative (red) or positive (green) experience. **c** Representative voltage responses to -100, -50, 0, 50 and 150 pA of step current injection in negative (red) and positive (green) engram cells. **d** Average firing frequency corresponding to current injection (FI curve) (negative engrams: n=10, positive engrams: n=17) . Error bars correspond to standard error and no point of the curve was significantly different between the two populations. **e-g** Suprathreshold characterization current-voltage responses of tagged hippocampal neurons. **e** FI gain is the slope of the linear part of the FI curve shown in D, calculated as the change in firing frequency from the minimum firing to maximum firing divided by the injected current. **h-i** Voltage and current step at which the neuron had at least one spike. **h** Adaptation ratio is calculated as the mean inter spike interval (ISI) during the last 200 ms of spiking divided the mean ISI during the first 200 ms of spiking during a current step corresponding to 20 Hz firing rate. **i**, Input resistance for each neuron, calculated by averaging 25 trials for change in voltage divided by 25 pA injected while holding the cell at -70 mV. **j-l** Analysis of spike shape of cells tagged by negative or positive experiences. **j** Spike traces from all the negative and positive cells (Bold trace corresponds to average trace shape). **k** Spike half width calculated as the time duration between two midpoints of the spikes. **l**, Deflection point of spike as identified by its first derivative. P-values were calculated based on independent t-test or Mann-Whitney test depending on normality of data.

Extended Data Fig. 5: Fluorescence counts for individual regions. Arbitrary units for EYFP (positive) and TdTom (negative) (N=3) for the **a,** anterior BLA (unpaired student's t-test t=7.279, df=4, p= 0.00019)**, b,** medial BLA (t=1.271, df=4; p= 0.2725)**, c,** posterior BLA (t=14.95, df=4; p=0.0001) **, d,** BMP (t=6.168, df=4; p=0.0035)**, e,** PFC (includes IL and PL) (t=1.078, df=4; p=0.3419), **f,** ACA (t=50.68, df=4; P<0.0001)**, g,** NAc Core (t=3.018, df=4; p=0.0392) **, h,** fornix (t=5.718, df=4; p=0.0046) **, i, hypothalamus** t=13.96, df=4; p=0.0002**, j,** upper layer of DG(t=54.94, df=4; p<0.0001)**, k,** lower layer of DG (t=11.73, df=4; p=0.0003).

Extended Data Fig. 6: RNA-seq analysis of hippocampus cells processing positive and negative memory engrams

aA Volcano plot with the relative fold change of gene expression in log 2 ratio and the FDR-adjusted p-value in log 2 ratio as X and Y axis showing the up and down regulated genes in positive vCA1 cells compared to negative vCA1 cells. Up or down regulated genes with FDR adjusted p-value less than 1e-5 plus at least four-fold differences were highlighted in either red or blue respectively. The gene names were displayed for the top 20 most significant protein coding genes as sorted by Wald statistics. b, Gene Set Enrichment Analysis of the up regulated pathways in positive engrams compared to negative engrams using Gene Ontology (GO) module. The size of the dot represents the gene count and the color of the dot indicates the FDR. Any pathway with a FDR smaller than 0.25 is considered as significantly enriched. c, GO analysis of down regulated pathways in positive engrams compared to negative engrams.

Extended Data Fig. 7: Terminal-specific optogenetic stimulation of vCA1 outputs leads to increased cFos in target areas

a, d, g, Representative images of ChR2-EYFP in BLA, NAc, and PFC terminals, respectively, and cFos expression after optical reactivation. **b, e, h**, Representative images of cFos without optogenetic reactivation of corresponding vCA1 terminals. **c, f, i**, Percent cFos/DAPI of BLA, NAc, and PFC non- stim vs stim groups (**P =0.0014, ****P < 0.0001 unpaired student's t-test)

Extended Data Fig. 8: Activating cells processing a neutral memory does not lead to changes in avoidance or preference. a Behavioral schedule in which vCA1 terminals are tagged in a neutral homecage experience (depicted as a yellow square during the off Dox period), followed by the induction protocol in which these outputs are activated concurrently during a positive experience in the BLA or NAc. Mice were injected with a virus cocktail consisting of cFos-tTa + TRE-ChR2-EYFP. **b-c** Percent preference for the stimulation side when optically activating vCA1 terminals over the **b**, BLA or **c,** NAc at 20Hz during baseline (D1), pre-induction (D2), and post-induction (D3) tests. d, Behavioral schedule in which vCA1 terminals are tagged in a neutral homecage experience and during induction are reactivated during a negative (shock) experience. **e-f** Percent preference for the stimulation side, neutral to negative, when optically activating vCA1 terminals over the **e,** BLA or **f,** NAc during D1, D5, and D7. NS = not significant; repeated measures one-way ANOVA followed by Tukey's multiple comparison test).

Extended Data Fig. 9: Terminal-specific optogenetic stimulation of vCA1 outputs did not affect distance travelled in all groups. Stimulation of vCA1 terminals over the **a**, BLA (n=8), **b**, NAc (n=10), or **c**, PFC (n=9), had no effect on the distance travelled between light on or off epochs and across pre-induction or post-induction timepoints.

Table S1: Top 20 up-regulated and downregulated genes in negative vs. neutral cells

SYMBOL	GENE NAME
Upregulated	
Ccl4	chemokine (C-C motif) ligand 4
Ccl3	chemokine (C-C motif) ligand 3
Ccl12	chemokine (C-C motif) ligand 12
Ucp3	uncoupling protein 3 (mitochondrial, proton carrier)
Slitrk2	SLIT and NTRK-like family, member 2
Etnppl	ethanolamine phosphate phospholyase
Ccl7	chemokine (C-C motif) ligand 7
Adgrb2	adhesion G protein-coupled receptor B2
Rnf225	ring finger protein 225
Cd48	CD48 antigen
Fam198a	golgi associated kinase 1A
Cst7	cystatin F (leukocystatin)
Drp2	dystrophin related protein 2
Gli1	GLI-Kruppel family member GLI1
Tnf	tumor necrosis factor
Luzp2	leucine zipper protein 2
Kcnj9	potassium inwardly-rectifying channel, subfamily J, member 9
Cxcl2	chemokine (C-X-C motif) ligand 2
Kcnj16	potassium inwardly-rectifying channel, subfamily J, member 16
Myoc	myocilin
Downregulated	
Ldlrap1	low density lipoprotein receptor adaptor protein 1
Rbpms2	RNA binding protein with multiple splicing 2
Fbxo30	F-box protein 30
Dvl3	dishevelled segment polarity protein 3
Gtpbp8	GTP-binding protein 8 (putative)
Usb1	U6 snRNA biogenesis 1
Mrps27	mitochondrial ribosomal protein S27
Slc16a11	solute carrier family 16 (monocarboxylic acid transporters), member 11
Wdr31	WD repeat domain 31
Mark1	MAP/microtubule affinity regulating kinase 1
Lrrc41	leucine rich repeat containing 41
Osbpl5	oxysterol binding protein-like 5
Matn2	matrilin 2
Pramef8	Putative PRAME Family Member 24

Ccdc17	coiled-coil domain containing 17
Exosc9	exosome component 9
Gprc5c	G protein-coupled receptor, family C, group 5, member C
Ttll1	tubulin tyrosine ligase-like 1
Gbe1	glucan (1,4-alpha-), branching enzyme 1
Fance	Fanconi anemia, complementation group E

Table S2: Top 20 upregulated and downregulated genes in positive vs. neutral cells

SYMBOL	GENE NAME
Upregulated	
Ccl4	chemokine (C-C motif) ligand 4
Ccl3	chemokine (C-C motif) ligand 3
Ccl12	chemokine (C-C motif) ligand 12
Etnppl	ethanolamine phosphate phospholyase
Papss2	3'-phosphoadenosine 5'-phosphosulfate synthase 2
Grik2	glutamate receptor, ionotropic, kainate 2 (beta 2)
Csmd2	CUB and Sushi multiple domains 2
Igdcc4	immunoglobulin superfamily, DCC subclass, member 4
F3	coagulation factor III
Kcnc4	potassium voltage gated channel, Shaw-related subfamily, member 4
Gria2	glutamate receptor, ionotropic, AMPA2 (alpha 2)
Rbp4	retinol binding protein 4, plasma
Slc1a2	solute carrier family 1 (glial high affinity glutamate transporter), member 2
Tnf	tumor necrosis factor
Phactr3	phosphatase and actin regulator 3
Gli1	GLI-Kruppel family member GLI1
Scg3	secretogranin III
Hrh1	histamine receptor H1
Ftmt	ferritin mitochondrial
Pdzph1	PDZ and pleckstrin homology domains 1
Downregulated	
Perp	PERP, TP53 apoptosis effector
Hemk1	HemK methyltransferase family member 1
Ppp4c	protein phosphatase 4, catalytic subunit
Hprt	hypoxanthine guanine phosphoribosyl transferase
Pcolce	procollagen C-endopeptidase enhancer protein
Sdf2l1	stromal cell-derived factor 2-like 1
Arf2	ADP-ribosylation factor 2
Trpv4	transient receptor potential cation channel, subfamily V, member 4

Evi5	ecotropic viral integration site 5
Fbxw11	F-box and WD-40 domain protein 11
Spint2	serine protease inhibitor, Kunitz type 2
Slc31a1	solute carrier family 31, member 1
Rfng	RFNG O-fucosylpeptide 3-beta-N-acetylglucosaminyltransferase
Tmem214	transmembrane protein 214
Eloa	elongin A
Ttc9	tetratricopeptide repeat domain 9
Ugdh	UDP-glucose dehydrogenase
Acd	adrenocortical dysplasia
Adsl	adenylosuccinate lyase
Zdhhc1	zinc finger, DHHC domain containing 1

Table S3: Top 20 upregulated and downregulated genes in positive vs. negative cells

SYMBOL	GENE NAME
Upregulated	
Ldlrap1	low density lipoprotein receptor adaptor protein 1
Nufip1	nuclear fragile X mental retardation protein interacting protein 1
Exosc9	exosome component 9
Pramef8	Putative PRAME Family Member 24
Gtpbp8	GTP-binding protein 8 (putative)
Commd10	COMM domain containing 10
Rnf113a1	ring finger protein 113A1
Cbr4	carbonyl reductase 4
Ndor1	NADPH dependent diflavin oxidoreductase 1
Fndc10	fibronectin type III domain containing 10
Gm20604	predicted gene 20604
Memo1	mediator of cell motility 1
Zdhhc12	zinc finger, DHHC domain containing 12
Eif4enif1	eukaryotic translation initiation factor 4E nuclear import factor 1
Phrf1	PHD and ring finger domains 1
Armc10	armadillo repeat containing 10
Tmco6	transmembrane and coiled-coil domains 6
Rgmb	repulsive guidance molecule family member B
Zfp524	zinc finger protein 524
Nxt1	NTF2-related export protein 1

Downregulated	
Arf2	ADP-ribosylation factor 2
Zfp386	zinc finger protein 386 (Kruppel-like)
Neu1	neuraminidase 1
Ppp4c	protein phosphatase 4, catalytic subunit
Gulp1	GULP, engulfment adaptor PTB domain containing 1
Ppp2r2b	protein phosphatase 2, regulatory subunit B, beta
Ccser2	coiled-coil serine rich 2
Zfp358	zinc finger protein 358
Eloa	elongin A
Gtpbp1	GTP binding protein 1
Evi5	ecotropic viral integration site 5
Cnep1r1	CTD nuclear envelope phosphatase 1 regulatory subunit 1
Ugdh	UDP-glucose dehydrogenase
Adsl	adenylosuccinate lyase
Perp	PERP, TP53 apoptosis effector
Stau2	staufen double-stranded RNA binding protein 2
Tmem214	transmembrane protein 214
Slc25a16	solute carrier family 25 (mitochondrial carrier, Graves disease autoantigen), member 16
Taf6	TATA-box binding protein associated factor 6
Rft1	RFT1 homolog

Figure 1

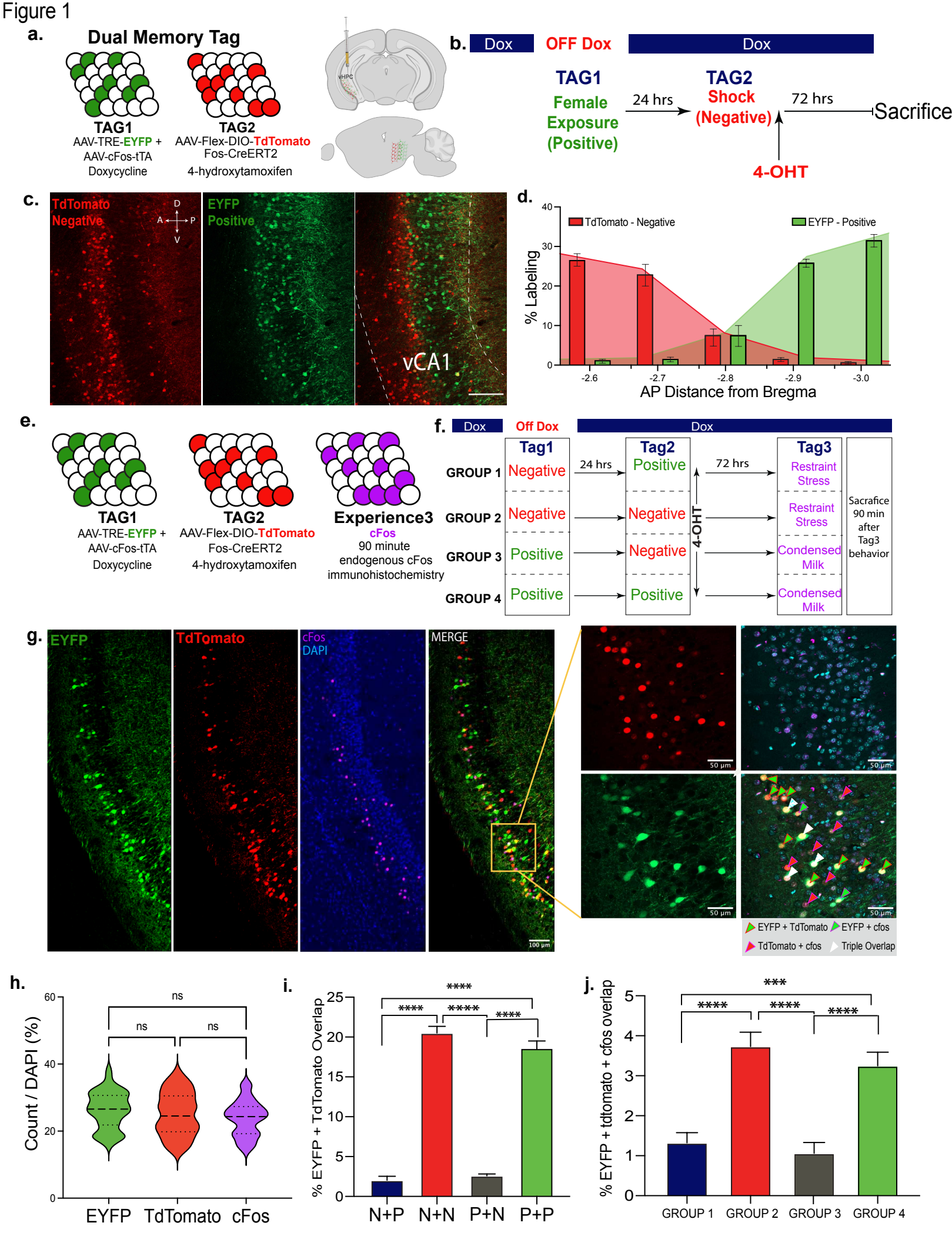
a.
Dual Memory Tag
TAG1
AAV-TRE-EYFP +
AAV-cFos-tTA
Doxycycline
TAG2
AAV-Flex-DIO-TdTomato
Fos-CreERT2
4-hydroxytamoxifen
vHPC
b.
Dox
OFF Dox
Dox
TAG1
Female Exposure (Positive)
24 hrs
TAG2
Shock (Negative)
72 hrs
Sacrifice
4-OHT
c.
TdTomato Negative
EYFP Positive
D
A
P
V
vCA1
d.
TdTomato - Negative
EYFP - Positive
% Labeling
AP Distance from Bregma
-2.6
-2.7
-2.8
-2.9
-3.0
e.
TAG1
AAV-TRE-EYFP +
AAV-cFos-tTA
Doxycycline
TAG2
AAV-Flex-DIO-TdTomato
Fos-CreERT2
4-hydroxytamoxifen
Experience3
cFos
90 minute
endogenous cFos
immunohistochemistry
f.
Dox
Off Dox
Dox
Tag1
Tag2
Tag3
GROUP 1
Negative
Positive
Restraint Stress
GROUP 2
Negative
Negative
Restraint Stress
GROUP 3
Positive
Negative
Condensed Milk
GROUP 4
Positive
Positive
Condensed Milk
24 hrs
72 hrs
4-OHT
Sacrifice 90 min after Tag3 behavior
g.
EYFP
TdTomato
cFos
DAPI
MERGE
100 µm
50 µm
EYFP + TdTomato
EYFP + cfos
TdTomato + cfos
Triple Overlap
h.
Count / DAPI (%)
ns
ns
ns
EYFP
TdTomato
cFos
i.
% EYFP + TdTomato Overlap
****
****
****
****
N+P
N+N
P+N
P+P
j.
% EYFP + tdtomato + cfos overlap
***
****
****
****
GROUP 1
GROUP 2
GROUP 3
GROUP 4

Figure 2

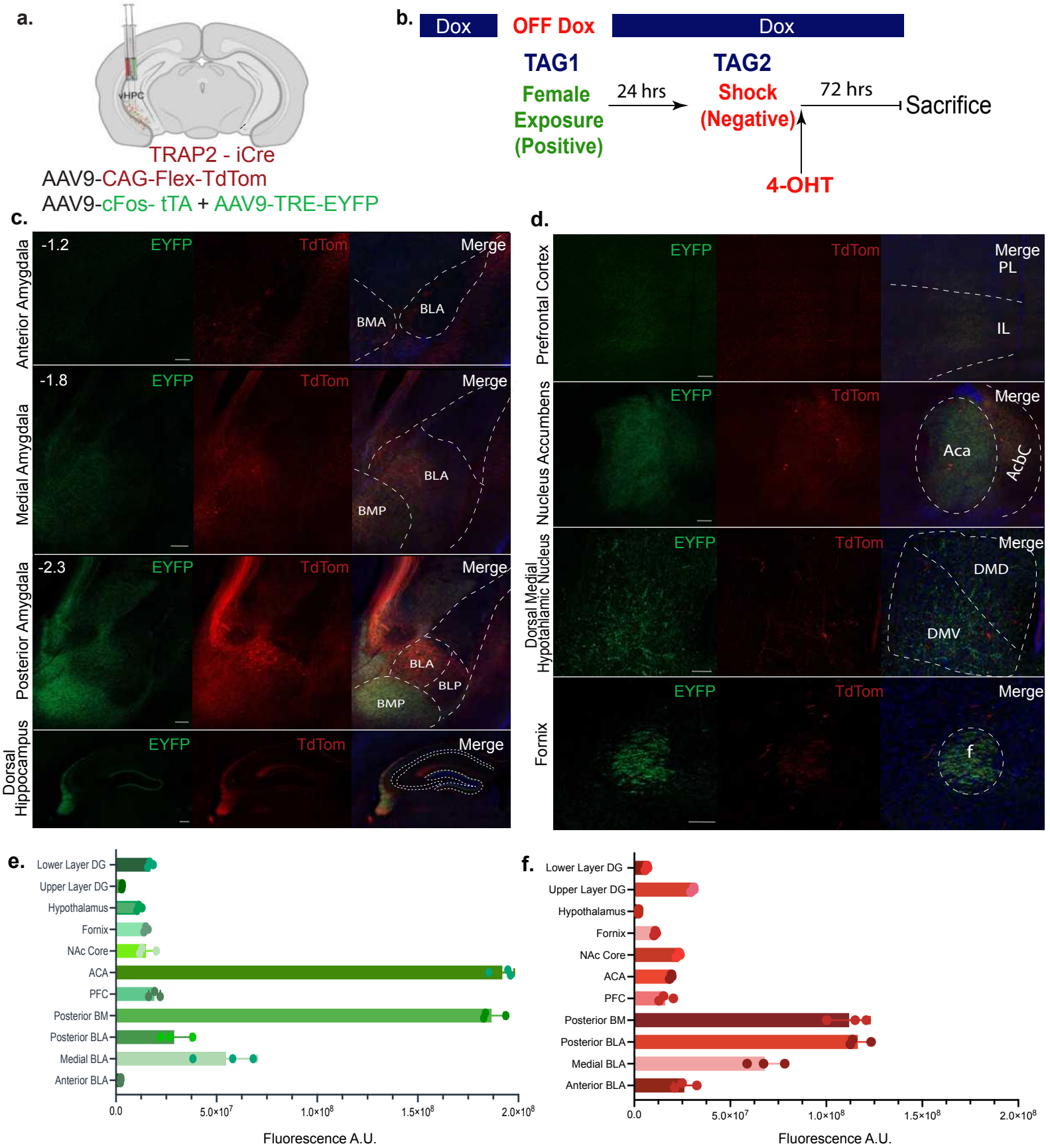
a.
vHPC
TRAP2 - iCre
AAV9-CAG-Flex-TdTom
AAV9-cFos- tTA + AAV9-TRE-EYFP
b.
Dox
OFF Dox
Dox
TAG1
Female Exposure (Positive)
24 hrs
TAG2
Shock (Negative)
72 hrs
Sacrifice
4-OHT
c.
Anterior Amygdala
Medial Amygdala
Posterior Amygdala
Dorsal Hippocampus
-1.2
-1.8
-2.3
EYFP
TdTom
Merge
BMA
BLA
BMP
BLP
d.
Prefrontal Cortex
Nucleus Accumbens
Dorsal Medial Hypothalamic Nucleus
Fornix
PL
IL
Aca
AcbC
DMD
DMV
f
e.
Lower Layer DG
Upper Layer DG
Hypothalamus
Fornix
NAc Core
ACA
PFC
Posterior BM
Posterior BLA
Medial BLA
Anterior BLA
0.0
5.0×10^7
1.0×10^8
1.5×10^8
2.0×10^8
Fluorescence A.U.
f.
Lower Layer DG
Upper Layer DG
Hypothalamus
Fornix
NAc Core
ACA
PFC
Posterior BM
Posterior BLA
Medial BLA
Anterior BLA
0.0
5.0×10^7
1.0×10^8
1.5×10^8
2.0×10^8
Fluorescence A.U.

Figure 3

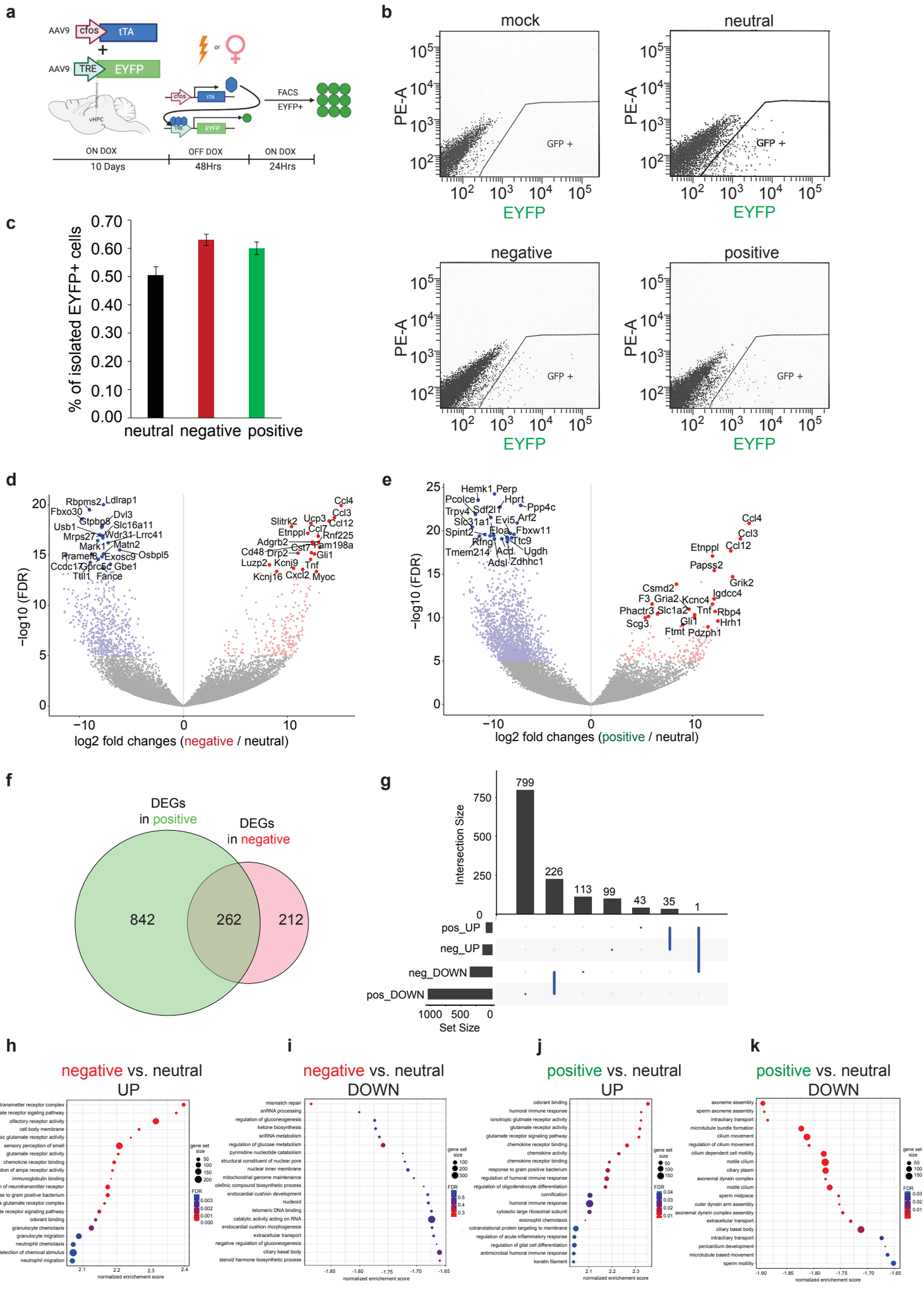
a
AAV9
cfos
tTA
AAV9
TRE
EYFP
vHPC
or
FACS
EYFP+
ON DOX
10 Days
OFF DOX
48Hrs
ON DOX
24Hrs
b
mock
neutral
negative
positive
PE-A
EYFP
GFP +
c
% of isolated EYFP+ cells
neutral
negative
positive
d
−log10 (FDR)
log2 fold changes (negative / neutral)
e
−log10 (FDR)
log2 fold changes (positive / neutral)
f
DEGs in positive
DEGs in negative
842
262
212
g
Intersection Size
Set Size
pos_UP
neg_UP
neg_DOWN
pos_DOWN
799
226
113
99
43
35
1
h
negative vs. neutral UP
i
negative vs. neutral DOWN
j
positive vs. neutral UP
k
positive vs. neutral DOWN
normalized enrichement score
gene set size
FDR

Figure 4

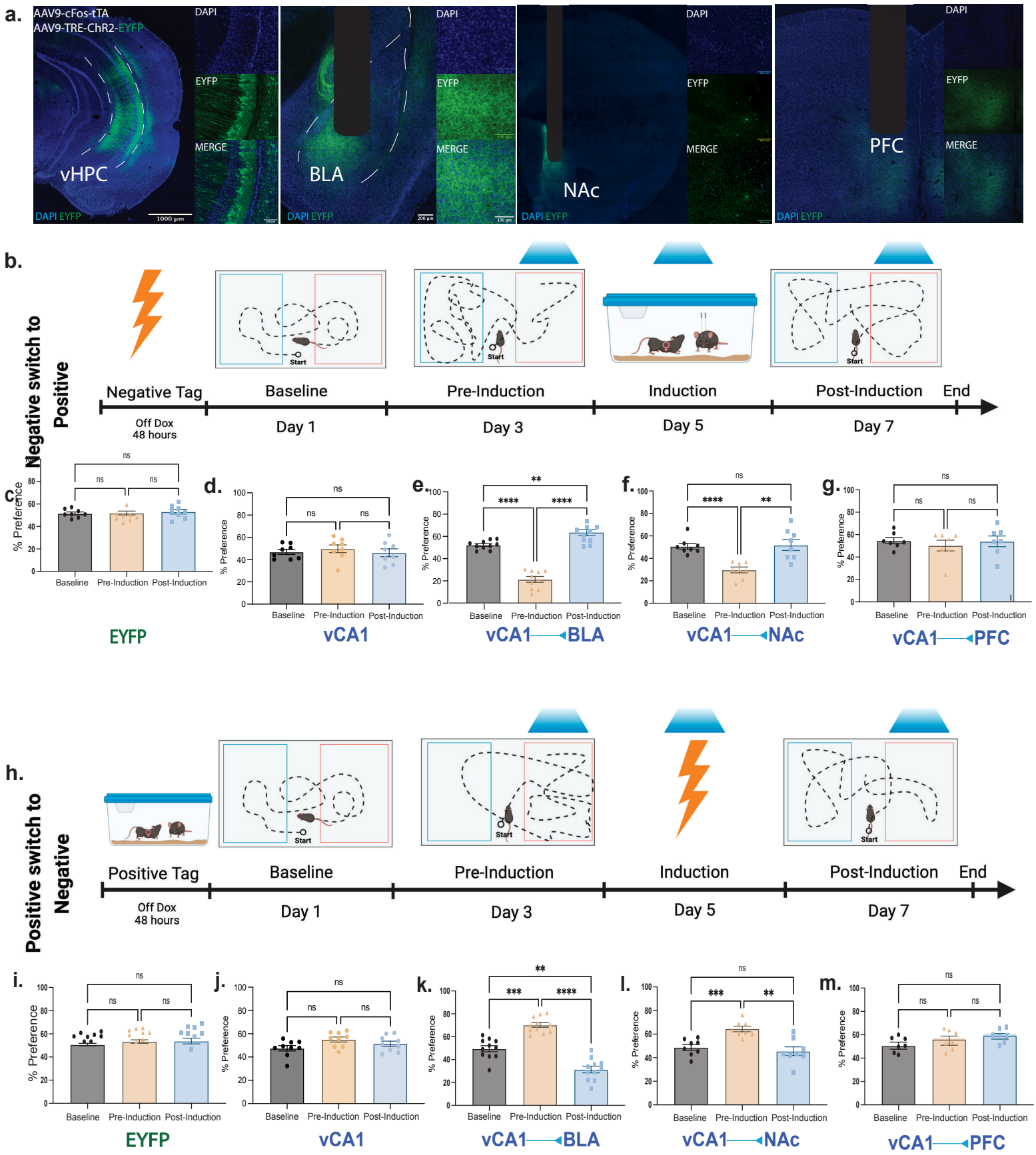
a.
AAV9-cFos-tTA
AAV9-TRE-ChR2-EYFP
DAPI
EYFP
MERGE
vHPC
BLA
NAc
PFC
DAPI EYFP
1000 µm
b.
Negative switch to Positive
Negative Tag
Off Dox 48 hours
Baseline
Day 1
Pre-Induction
Day 3
Induction
Day 5
Post-Induction
Day 7
End
Start
c.
d.
e.
f.
g.
% Preference
Baseline
Pre-Induction
Post-Induction
ns
**
****
EYFP
vCA1
vCA1 BLA
vCA1 NAc
vCA1 PFC
h.
Positive switch to Negative
Positive Tag
i.
j.
k.
l.
m.
***

Extended Data Fig. 1

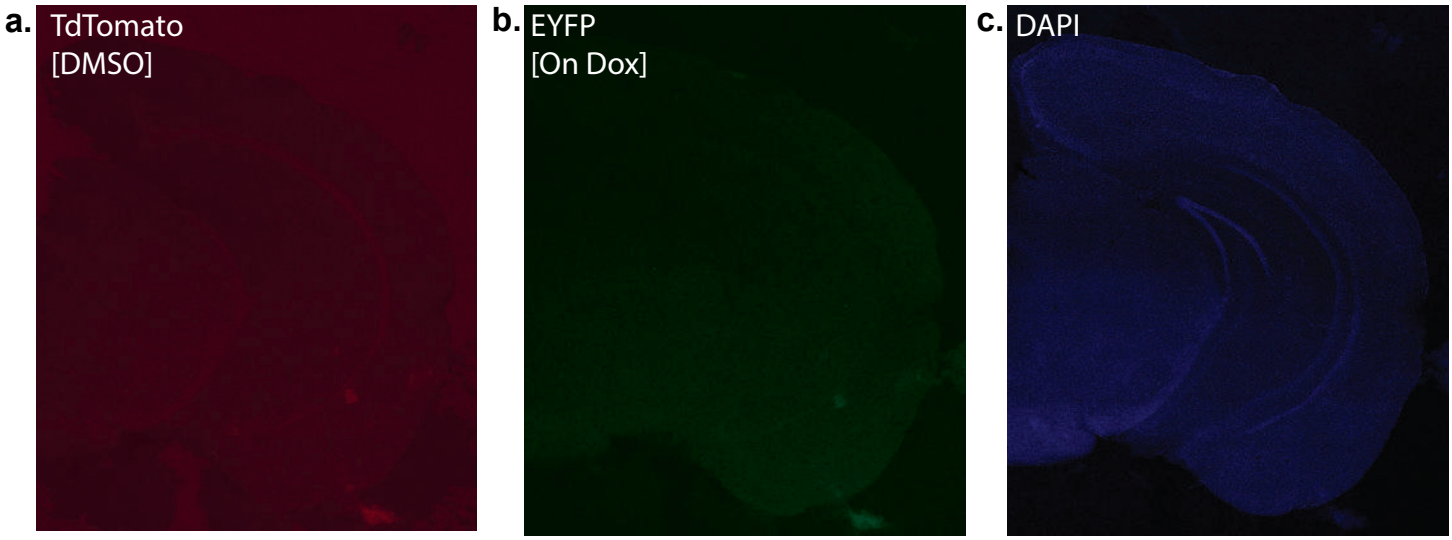

Extended Data Fig. 2

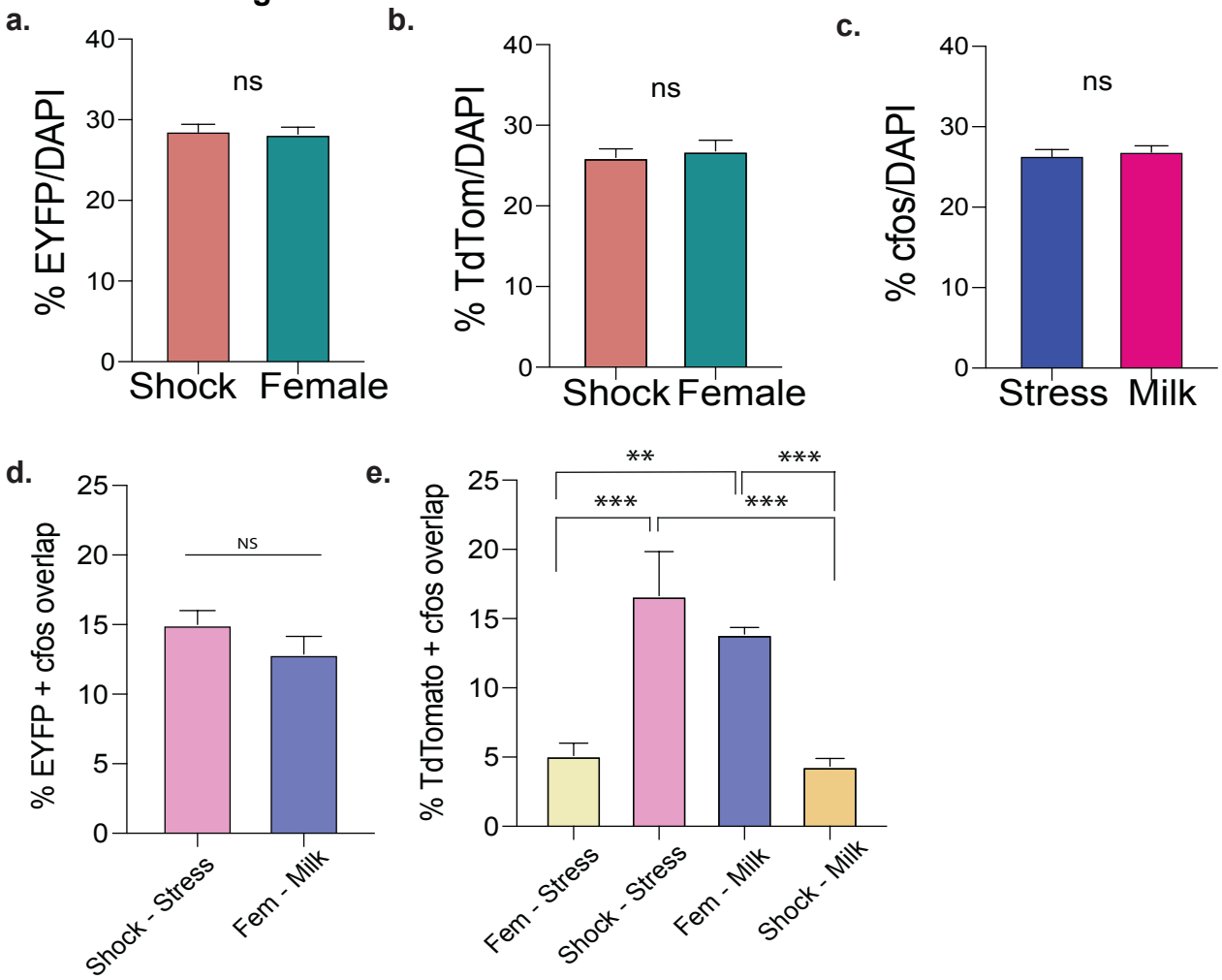

Extended Data Fig. 3

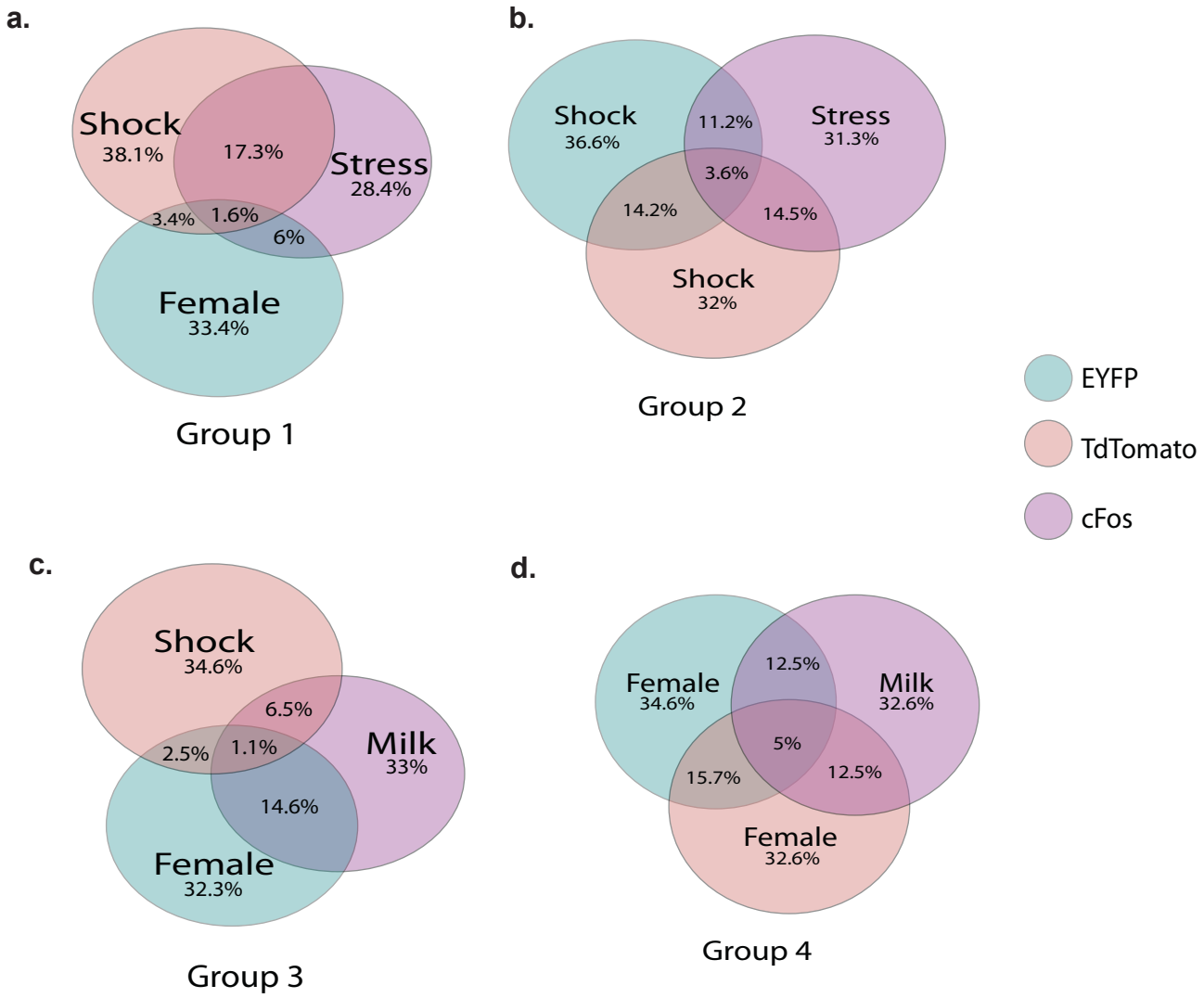

Extended Data Fig. 4

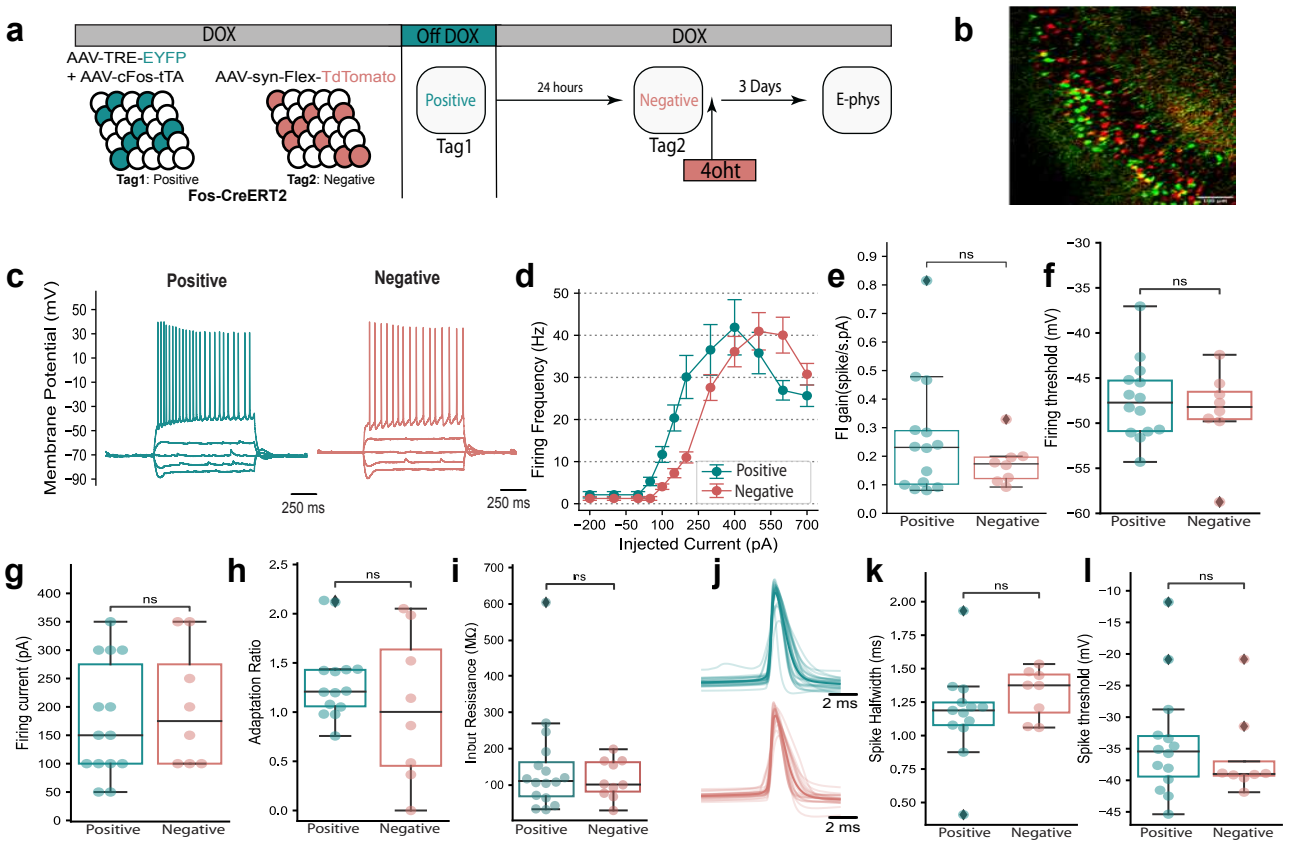

Extended Data Fig. 5

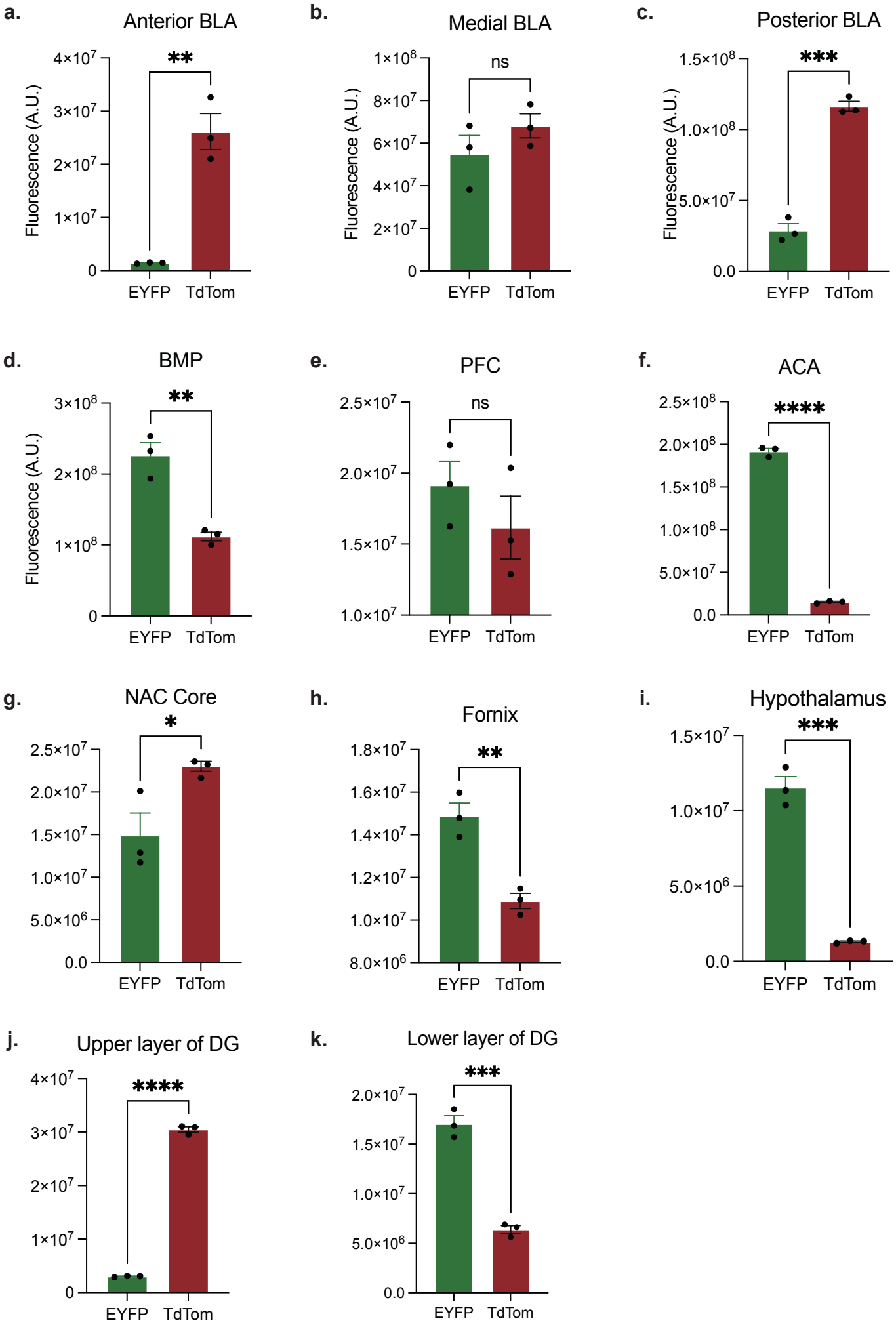

Extended Data Fig. 6

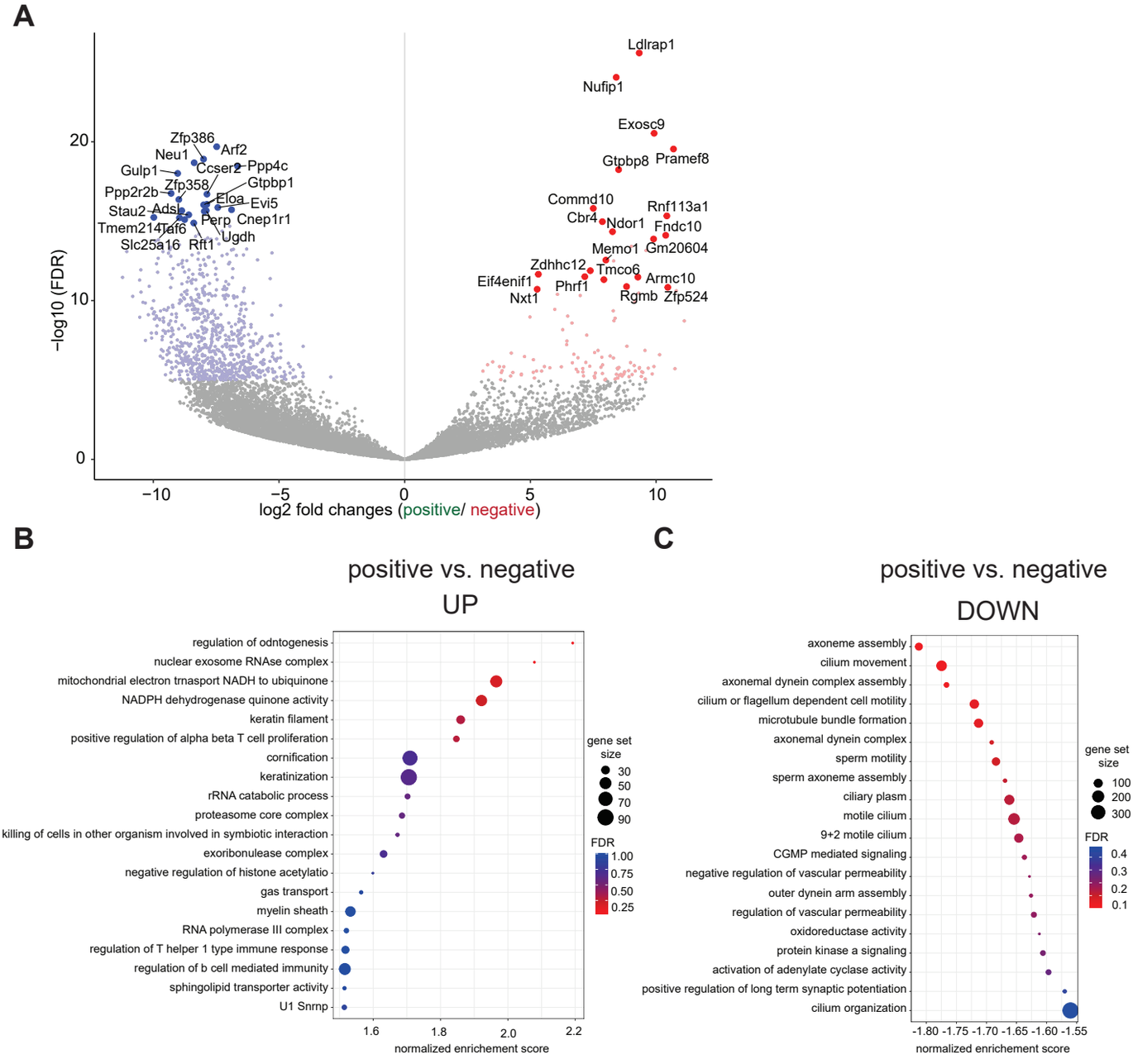

Extended Data Fig. 7

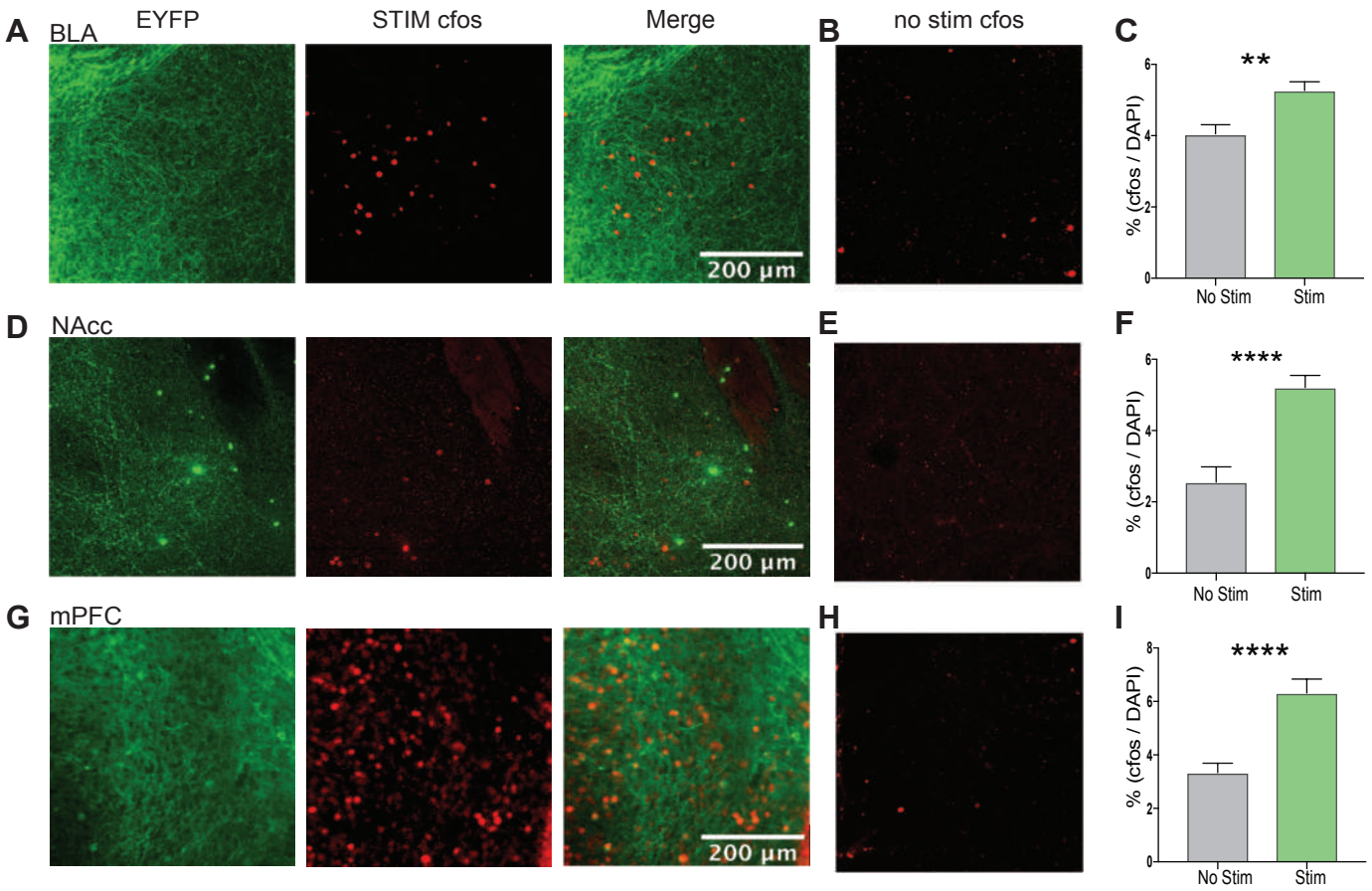

Extended Data Fig. 8

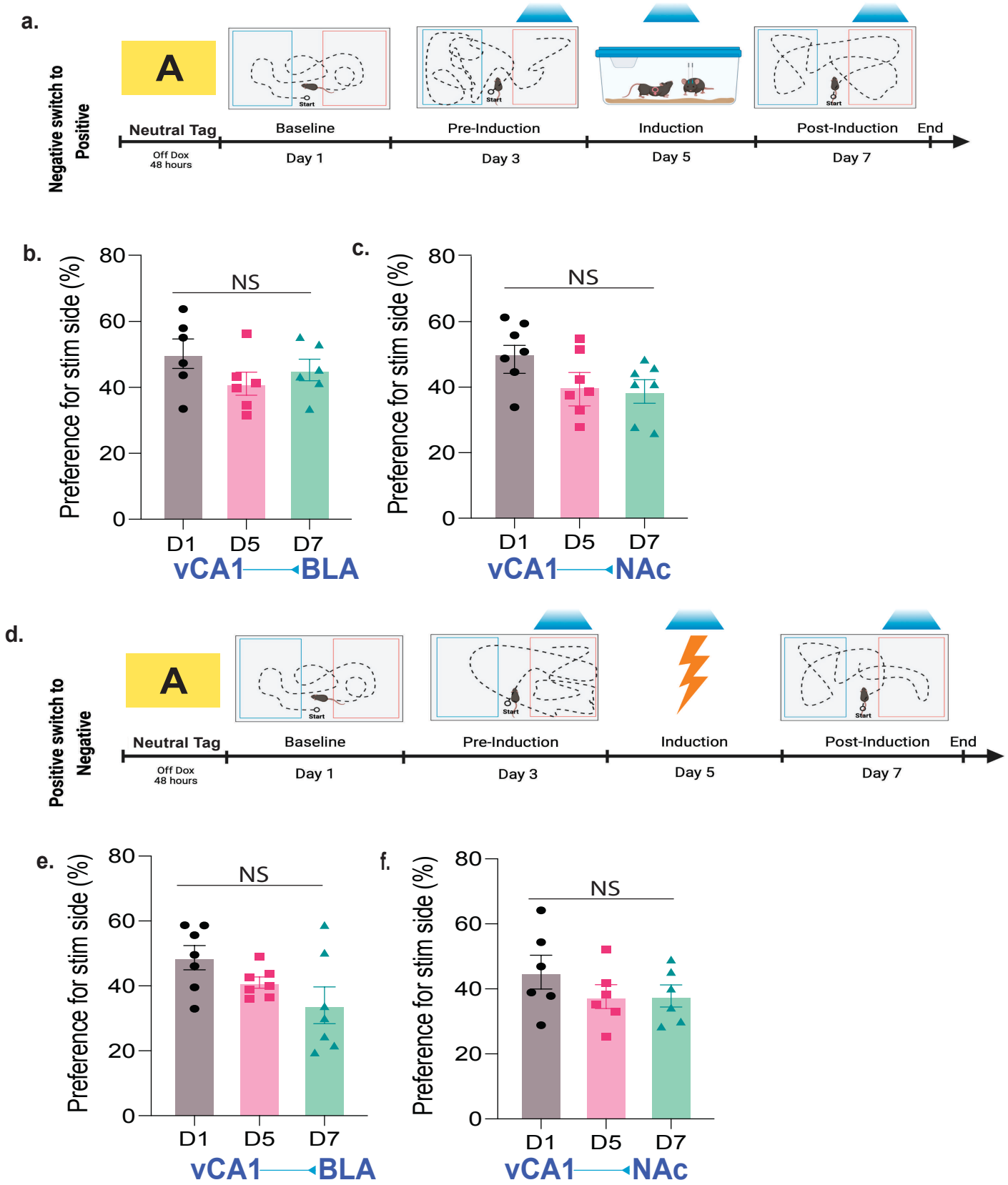
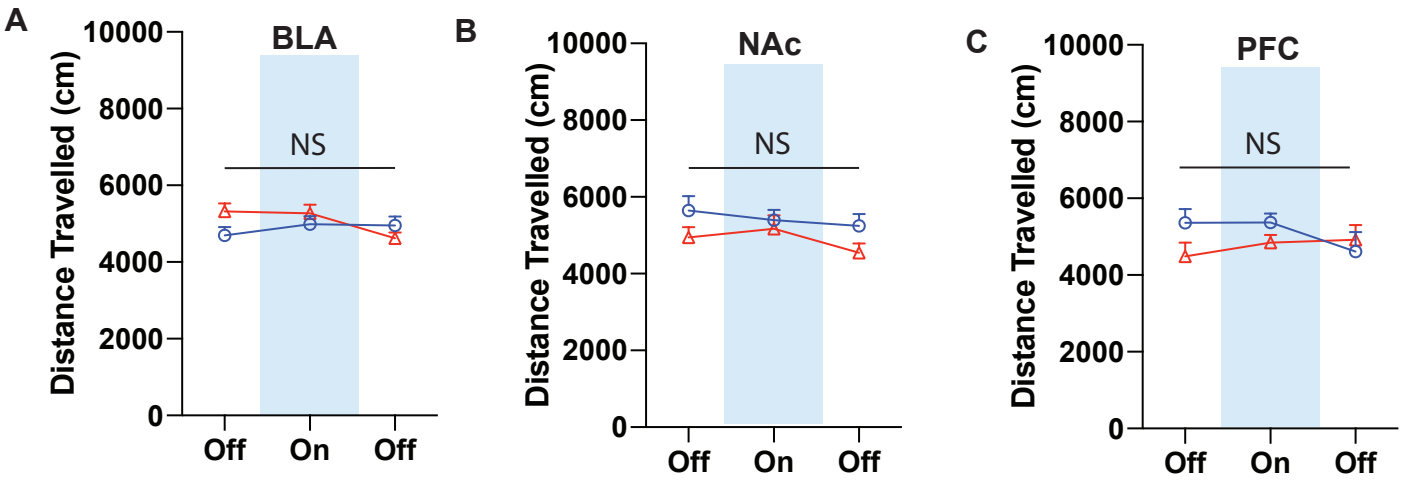
Extended Data Fig. 9